AN ABSTRACT OF THE THESIS OF

Arash Abbasi for the degree of Doctor of Philosophy in
Electrical and Computer Engineering presented on Decemeber 7, 2015.

Title: Ultra-wideband Relay Commuincation Systems

Abstract approved: _____

Huaping Liu

Impulse-radio ultra-wide-band (IR-UWB) signaling is a promising technique for high-speed, short-range relay communications networks. Depending on how the relay node retransmits the signal, there are two main relay schemes: conventional one-directional (one-way) relay model, and bi-directional (two-way) relay model. In bi-directional relay communications, wireless network coding (WNC), also called physical-layer network coding (PNC), could be applied to overcome the spectral efficiency limitation of the conventional one-way relay.

In the first part of this work, we propose asynchronous, differential, and bidirectional decode and forward (ADBDF) and asynchronous, differential, and bidirectional denoise and forward (ADBDNF) UWB relay methods, where the relay node (RN) does not need to be synchronized with the end nodes (ENs). The proposed schemes are attractive for networks in which stringent/complicated synchronization between the RN and the ENs may not be feasible.

The second part of this work focuses on UWB channel classification. We propose a 2-dimensional (2-D) LOS/NLOS classification scheme that uses skewness

of the channel impulse/pulse response. The proposed channel classification decreases the complexity of existing channel classification methods and can be used in a variety of areas such as localization, relay communications, and cooperative communications.

The final part of this work deals with compressive sensing (CS) algorithms that employ sub-Nyquist sampling for UWB communications. We develop coarse graining (CG) for the proposed CS sub-Nyquist sampling technique, which leads to: (1) reduced sampling rate at the receiver, and hence reduced use of analog-to-digital converters (ADCs) resources; and (2) low-complexity channel estimation.

Ultra-Wideband Relay Communication Systems

by

Arash Abbasi

A THESIS

submitted to

Oregon State University

in partial fulfillment of
the requirements for the
degree of

Doctor of Philosophy

Presented Decemeber 7, 2015
Commencement June 2016

Doctor of Philosophy thesis of Arash Abbasi presented on Decemeber 7, 2015.

APPROVED:

Major Professor, representing Electrical and Computer Engineering

---

Director of the School of Electrical Engineering and Computer Science

---

Dean of the Graduate School

I understand that my thesis will become part of the permanent collection of Oregon State University libraries. My signature below authorizes release of my thesis to any reader upon request.

Arash Abbasi, Author

ACKNOWLEDGEMENTS

I would never have been able to finish my dissertation without the guidance of my advisor, support from my parents, my brothers and my sister.

I would like to express my deepest gratitude to my advisor, Prof. Huaping Liu, for his excellent guidance, invaluable advice, continuous encouragement and financial support. Without his help, I cannot finish this dissertation successfully. I am also very thankful to his understanding and caring to my study and life.

I would like to thank my parents, my sister and my brothers. They are always supporting me and encouraging me with their best wishes. This dissertation is dedicated to them.

TABLE OF CONTENTS

TABLE OF CONTENTS (Continued)

TABLE OF CONTENTS (Continued)

LIST OF FIGURES

LIST OF FIGURES (Continued)

LIST OF TABLES

Chapter 1 – Introduction

1.1 Overview

Ultra-wideband (UWB) radios have the potential to increase the spectrum-use efficiency [1]. However, because of the strict regulations on the transmitted power of UWB signals, these systems face some challenges in achieving wide coverage while assuring an adequate system performance [2]. These drawbacks should be solved for the widespread deployment of UWB systems. Recently, cooperative diversity has emerged as an effective scheme to overcome multi-path fading in wireless networks. The basic idea of the cooperative strategy is to transmit data through multiple nodes in the network and these nodes work cooperatively to improve the overall network performance by the provided diversity.

There are three main challenges in UWB relay communication systems: (1) coherent synchronous detection/demodulation schemes are prohibitively complex; (2) non-line-of-sight (NLOS) propagation significantly degrades the performance; and (3) analog-to-digital converters (ADCs) working at the Nyquist rate are expensive and power hungry.

This dissertation focuses on addressing these problems and develops algorithms to classify LOS/NLOS UWB channels, improve UWB relay communication systems performance and finally decrease the high sampling rate required for UWB signals.

1.2 Summary of Contribution

First, we propose a 2-dimensional (2-D) LOS/NLOS classification scheme that uses skewness of the channel impulse/pulse response, which has not been used by existing work. While extensive work in this area exists, one channel statistical parameter which has not been used in existing work is the skewness of the channel impulse response (CIR) or channel pulse response (CPR). Since skewness characterizes the amount and direction of skew (departure from horizontal symmetry), it could be an effective parameter for LOS/NLOS classification; if the skewness of the impulse response of a UWB channel is high, then the channel is more likely to be LOS and vice versa.

Second, asynchronous, differential, and bidirectional UWB relay schemes are developed. The proposed algorithms are suitable for UWB communication systems where maintaining a synchronous link between the relay node (RN) and the end nodes (ENs) with coherent demodulation/detection, as commonly assumed in existing work, is difficult and expensive. Two novel asynchronous differential bidirectional decode and forward (ADBDF) and asynchronous differential bidirectional denoise and forward (ADBDNF) algorithms are proposed in which the relay is not required to be synchronized with the ENs. Additionally, a closed-form expression for solving integrals involving the Gaussian Q-function is presented which can be conveniently used to calculate the average of the error probability in fading channels.

Finally, we propose a coarse graining (CG) technique in compressive sensing (CS) theory which can be employed in UWB channel estimation algorithms. The proposed method would be useful when a low-complexity and fast channel

estimation/synchronization is desired. We derive a closed-form expression for applying the CG technique in CS-UWB channel estimation algorithm. We also derive a closed-form ℓ_1-optimization expression for the proposed UWB channel estimation, and study the performance of the proposed method for different UWB LOS/NLOS indoor environments.

1.3 Dissertation Outline

Chapter 2 briefly reviews UWB communications systems and different UWB channel types.

In chapter 3, different UWB relay communication techniques are described and the advantages and disadvantages of each technique are analyzed. Then we introduce two UWB relay communication algorithms that are suitable for low-complexity fast applications to improve the coverage of the localization and the throughput.

In chapter 4, UWB channel classification/identification techniques are studied. The effects of NLOS propagation in different UWB communication systems are investigated. We then present a scheme that uses skewness for LOS/NLOS channel classification. We also analytically derive the performance of the method that employs skewness.

In chapter 5, CS theory and sub-Nyquist sampling theorem for UWB communication systems are investigated. We propose a CG algorithm which can be applied in CS to further decrease the sampling rate.

Chapter 6 gives conclusions and future work.

1.4 Notation

$\approx$	approximately equals to
$\|.\|_p$	ℓ_p-norm
$\mathrm{Tr}(\cdot)$	the trace of a matrix
$\mathrm{E}\{\cdot\}$	the expectation
$\ll$	much small than
$\stackrel{\Delta}{=}$	is defined as being equal to
$\boldsymbol{I}_m$	$m \times m$ identity matrix

1.5 Abbreviations

CS	Compressive sensing
CG	Coarse graining
UWB	Ultra wideband
2-D	Two-dimensional
3-D	Three-dimensional
AWGN	Additive white Gaussian noise
NLOS	Non-line-of-sight
LOS	Line-of-sight
RMSE	Root mean-square error
ML	Maximum likelihood
RN	Relay node
EN	End node
FCC	Federal communications commission
ns	Nanosecond
BER	Bit error rate
PER	Packet error rate
CIR	Channel impulse response
FRI	Finite rate of innovation
ADC	Analog-to-digital converters
ADBDF	Asynchronous differential bidirectional decode and forward
ADBDNF	Asynchronous differential bidirectional denoise and forward
WNC	Wireless network coding
PNC	Physical-layer network coding
AF	Amplify and forward
DF	Decode-and-forward
APDP	Average power delay profile
MUI	Multi user interference
MLSD	Maximum likelihood sequence detection
NNUB	Nearest neighbor union bound

Chapter 2 – Ultra-wideband Preliminaries

This chapter provides an overview of UWB communications systems. A mathematical representation of UWB signals/channels is reviewed. Also, the advantages and features of UWB communication systems are summarized.

2.1 UWB Definition

Impulse radio UWB (IR-UWB) has the potential to provide high data rates, fine time resolution, multipath immunity and coexistence with legacy services via frequency overlay. Thus, it is a good candidate for short range connectivity, location-aware wireless sensor networks and low-rate communications with ranging capability [1–8]. IR-UWB systems convey information by transmitting short-duration pulses, typically in the range of sub-nanoseconds to nanoseconds. The federal communications commissions (FCC) in 2002 defines UWB as having a fractional bandwidth greater than 20% or an absolute bandwidth of at least 500 MHz. The absolute bandwidth is calculated as the difference between the upper frequency f_H of the -10 dB emission point and the lower frequency f_L of the -10 dB emission point, which is also called -10 dB bandwidth, as shown in Fig. 2.1. The fractional bandwidth is defined as $B_{frac} = \frac{B}{f_c}$ and $B = f_H - f_L$. In this case the fractional bandwidth can be rewritten as

$$B_{frac} = \frac{2(f_H - f_L)}{f_H + f_L}. \tag{2.1}$$

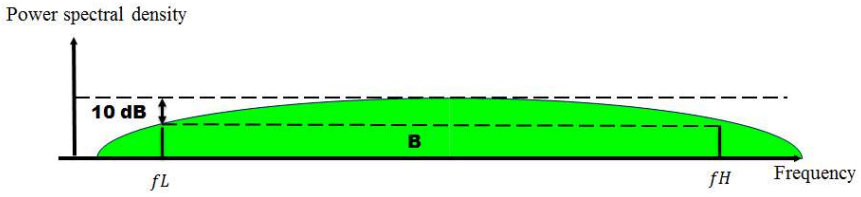

Figure 2.1: Illustration of UWB definition.

2.2 FCC Regulations for UWB Signals

Since UWB systems need to coexist with other legacy narrow band systems, the transmission power of the UWB devices is strictly limited so that the UWB signals have negligible effects on the pre-existing narrow band systems. Specifically, the average power spectral density (PSD) cannot exceed -41.3 dBm/MHz over the frequency band from 3.1-10.6 GHz, and it is even lower outside this band, depending on the specific application. For indoor and outdoor UWB communication systems, the FCC limits are shown in Fig. 2.2. The only difference in the limit between the outdoor and indoor systems is that the emission for outdoor systems in the frequency band from 1.61-3.1 GHz and 10.6-15 GHz should have an extra attenuation of 10 dB compared to that of indoor systems. Besides the FCC emission limit, there are some other common FCC regulations for all the UWB systems [25, 26].

- The frequency f_M at which the highest power is emitted must be within the -10 dB absolute signal bandwidth.

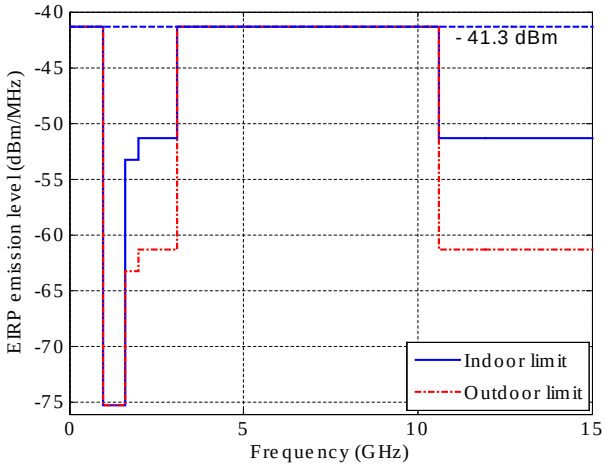

Figure 2.2: FCC emission limits for indoor and outdoor UWB communication systems.

- Peak emissions within a 50 MHz bandwidth around f_M may not exceed 0 dBm EIRP.
- Operation on aircraft, ship, or satellite is not permitted.

2.3 UWB Standard

There have been efforts to establish standards to provide compliance between devices from different origins. One of the leading standardization organizations is the IEEE LAN/MAN Standards Committee. IEEE 802.15 Task Groups 3 and 4 established standards for wireless personal area networks (WPAN), which led to IEEE-Std 802.15.3 for high-data rate [9] and IEEE-Std 802.15.4 for low-data rate [10]. The IEEE-Std 802.15.3a proposal for high-data-rate has led to the multi-band (MB)-OFDM UWB approach, which became the de facto stan-

dard for high-data rate UWB communications, and was later adopted by the WiMedia alliance for certified wireless-USB. MB-OFDM is a carrier based communication protocol that divides the 3.1-10.6 GHz UWB spectrum into 14 bands of 528 MHz each [11–14]. The MB-OFDM approach has been primarily used for applications such as streaming video and wireless USB with data rates of 480Mb/s. A second outcome of the 802.15.3a task group was a direct sequence (DS) UWB standard, supported by the UWB Forum (this is more in the original spirit of UWB transmission of very narrow pulses, from 100 ps to 1 ns, and considering a low frequency band from 3.1-5.15 GHz and a high frequency band between 5.825-10.6 GHz). The IEEE-Std 802.15.4a proposal for low-data rate [10] also considered the division into a lower band (3.1-5 GHz) and an upper band (6-10.6 GHz). The IEEE 802.15 Task Group 6 (IEEE 802.15.6) was formed in Nov. 2007 and is currently developing a communication standard for body area networks (BAN). A heterogeneous approach of IR-UWB signaling paired with narrowband signaling is being considered for this standard. IR-UWB radios, however, can be designed with relatively low complexity and low power consumption. They have therefore found a niche in energy constrained, short-range wireless applications including personal-area-networks, low-power sensor networks, and wireless body-area-networks. Because of the bandwidths that can be achieved with IR-UWB radios, they are also used in precise location systems and for dedicated high-data-rate communication links. IR transmits information by altering the positioning, amplitude, presence of pulse, or shape of the UWB pulse, which corresponds to pulse position modulation (PPM), pulse amplitude modulation (PAM), on-off keying (OOK), or pulse shape modulation (PSM), respectively. The continuous transmission of uniformly spaced pulses gives rise

to strong spectrum spikes occurring at integer multiples of the pulse repetition frequency. Therefore, time hopping (TH) and direct sequence (DS) techniques can be adopted to mitigate the frequency spikes by randomizing the pulse train. TH and DS can also enable multiple access in UWB systems. TH is often applied to low data rate UWBs with low pulse duty cycles. DS is suitable for medium to high data rate transmissions with high duty cycles. Many IR-UWB applications concern short-to-medium range with low data-rate and are focused on achieving low power consumption. Applications that have been considered include wireless sensor networks, sensing and positioning [15–17] systems, inter-chip communication [18,19] contactless wireless [20], biological or biomedical networks [21,22], and imaging systems [23]. The main advantages can be summarized as follows:

- Good ability to penetrate through obstacles;
- High precision ranging, and hence high positioning accuracy;
- Potentially low power consumption.

The penetration capability of the UWB signal is due to its large frequency spectrum that includes low frequencies as well as high frequencies. The large bandwidth also results in a high time-resolution, which improves the ranging accuracy.

2.4 UWB Channel Preliminaries

Due to the huge bandwidth of UWB signals, the channel is different from narrowband wireless channels. UWB channels are characterized by the dense multipath that come in clusters. The UWB channel is usually studied by extracting

a statistical model from measurements. Parameters of the model reflect the statistical properties of various propagation environments. We adopt the multi-path channel model specified by the IEEE 802.15.4a group for the performance evaluation of the physical layer. The impulse response with this model can be expressed mathematically by [12]

$$h(t) = \tilde{\beta} \sum_{r=0}^{R-1} \sum_{k=0}^{K-1} b_{k,r} e^{j\phi_{m,l}} \delta(t - T_r - \tau_{k,r}), \tag{2.2}$$

where $b_{k,r}$ is the gain of the k-th path in the r-th cluster, R is the number of clusters, K is the number of rays in each cluster, T_r is the delay of the r-th cluster, and $\tau_{k,r}$ is the delay of the k-th ray in r-th cluster [24]. The factor $\tilde{\beta}$ jointly models the pathloss and shadowing. Cluster arrival time in UWB CIR is modeled by a Possion process

$$p\left(T_r | T_{(r-1)}\right) = \Lambda \exp\left[-\Lambda\left(T_r - T_{(r-1)}\right)\right], \tag{2.3}$$

where Λ is the cluster arrival rate [24]. Furthermore, in order to fit better for most environments, within each cluster, the distribution of the ray arrival times is modeled by the mixture of two Poisson processes

$$\begin{aligned} p\left(\tau_{k,r} | \tau_{(k-1),r}\right) =& \beta\lambda_1 \exp\left[-\lambda_1\left(\tau_{k,r} - \tau_{(k-1),r}\right)\right] \\ &+ (1-\beta)\,\lambda_2 \exp\left[-\lambda_2\left(\tau_{k,r} - \tau_{(k-1),r}\right)\right], \end{aligned} \tag{2.4}$$

where β is the mixture probability of two Poisson distributions with λ_1 and λ_2 ray arrival rates, which take different values in LOS/NLOS environments [24]. The distribution of the small-scale fading, i.e., $b_{k,r}$ in (2.2), is Nakagami

with parameter $m_{k,r}$, which is modeled as a lognormally distributed random variable, and finally the phase $\phi_{k,r}$ is considered as a uniformly distributed random variable over $[0, 2\pi]$. The detail of the joint probabilistic model of these parameters is summarized in [24].

Chapter 3 – Compressive Sensing Sub-Nyquist Sampling With Coarse Graining

3.1 Introduction

Wireless communications using a very large bandwidth face some common technical challenges: (1) ADCs working at the Nyquist rate are in general very expensive and power hungry; (2) timing synchronization at sub-nanosecond precision is difficult to accomplish; and (3) exploiting multipath diversity by capturing sufficient number of paths needs accurate channel estimation.

Since IR-UWB signals are known to have resolvable multipath with sparse structure at the receiver, the application of compressive sensing theory for UWB channel estimation appears to be attractive, which leads to: (1) reduced sampling rate at the receiver, and hence, reduced use of ADCs resources; and (2) low-complexity channel estimation and timing synchronization. CS theory asserts that the number of measurements (samples) needed to reconstruct a signal without error depends on its sparsity and not purely on the bandwidth [27–32]. Hence, if a signal has a sparse representation in some domains, for example time or frequency, it is possible to recover the signal with a high probability from a set of random linear projections using nonlinear reconstruction algorithms.

In this chapter the basics of CS and sub-Nyquist sampling theory are explained first. The CG technique for CS UWB channel estimation is developed

in Sec. 3.5. The effects of the proposed algorithms for different LOS/NLOS IEEE 802.15.4a UWB channel models are investigated in Sec. 3.6.

3.2 Innovation Rate for UWB Signals

Inspired by the fact that the received UWB signals are made up of many pulses among which only a few are dominant components appearing at different points in time, can we estimate only these dominant components? To answer this question, we apply a CG technique in UWB channel estimation which provides a means to study complex systems (in our case, UWB channels) by smoothing away the fine details of the full explicit systems such that we only estimate the dominant components.

Innovation rate for a signal is defined as the number of degrees of freedom in representing the signal per unit of time. Vetterli *et al.* [33, 34] showed that non-bandlimited signals with finite rate of innovation (FRI) can be recovered from uniform sub-Nyquist sampling. An example of FRI signal class is the UWB signal which we aim to investigate in this section. UWB CIR can be modeled as one period of the following τ-periodic signal

$$x(t) = \sum_{k' \in \mathbb{Z}} \sum_{k=0}^{K-1} b_k \delta(t - t_k - k'\tau), \tag{3.1}$$

where b_k is the gain of k-th delta function and k-th delta function is located at $t_k \in [0, \tau]$. In this case, the innovation rate is the average number of delta functions per unit of time: $\rho = \lim_{T \to \infty} \frac{C_T}{T}$, where C_T is the number of delta functions in the interval $[-T/2, T/2]$.

As commonly adopted, the cluster arrival rate and the ray arrival rate are independent. Also the values of R and K tend to infinity. In this case, from (2.3) the innovation rate for the UWB channel can be calculated as

$$\rho = 2\Lambda\left(\beta\lambda_1 + (1-\beta)\,\lambda_2\right). \tag{3.2}$$

If signal $x(t)$ in (3.1) is filtered by a low-pass filter $\psi(t)$ with a bandwidth of B where $B \geq 2K/\tau = \rho$, and then sampled uniformly at N locations, where $N > B\tau$ and $T = \tau/N$, these samples are sufficient for characterizing $x(t)$. An example of the low-pass filter is [33]

$$\psi(t) = \frac{sin\left(\pi Bt\right)}{B\tau sin\left(\pi t/\tau\right)}. \tag{3.3}$$

The above procedure can also be applied to non-periodic UWB signals. If the received UWB signal $y(t)$ is filtered by an ideal bandpass filter $H_b = \sqcap\left(\omega_1, \omega_2\right)$, and sampled uniformly at sub-Nyquist rate $f_s \geq \left(\omega_2 - \omega_1\right)/2\pi$, then the N samples of $Y(\omega)$ with step $\omega_0 = \frac{\omega_2 - \omega_1}{N-1}$ and $N \geq 2L$

$$Y[n] = Y(\omega_n) = Y\left(\omega_1 + (n-1)\omega_0\right), \quad n = 1, 2, \cdots, N, \tag{3.4}$$

are a sufficient characterization of $y(t)$. The above procedure is still applicable for time-limited non-periodic UWB signals. In practice, discrete Fourier transform (DFT) coefficients are computed to calculate the frequency response. Let

$Y_a[n] = Y[n]/S[n]$. In this case we have

$$Y_a\left[n\right] = \sum_{l=0}^{L-1} b_l e^{-j\omega_n \tau_l} + \eta\left[\omega_n\right], \tag{3.5}$$

where $\eta[\omega_n] = \mathcal{N}[\omega_n]/S[\omega_n]$. In the absence of noise, the exponential term $\left\{e^{-j\omega_n\tau_l}\right\}_{n\in\mathbb{Z}}$ can be annihilated by a FIR filter like $H(z) = \prod_{l=0}^{L-1}\left(1 - e^{-j\omega_0\tau_l}z^{-1}\right) = \sum_{l=0}^{L-1} H[l]z^{-l}$, that is

$$\begin{aligned} H[n] * Y_a[n] &= \prod_{l=0}^{L-1}\left(\delta[n] - e^{-j\omega_0\tau_l}\delta[n-1]\right) * \sum_{l=0}^{L-1} b_l e^{-j\omega_n\tau_l} \\ &= \prod_{l=0}^{L-1}\sum_{l=0}^{L-1} b_l\left(e^{-jn\omega_0\tau_l} - e^{-j(n-1)\omega_0\tau_l}e^{-j\omega_0\tau_l}\right) \\ &= \prod_{l=0}^{L-1}\sum_{l=0}^{L-1} b_l \times 0 = 0 \end{aligned} \tag{3.6}$$

where * denotes convolution.

The above equation can be represented in matrix form as

$$\begin{pmatrix} Y_a[L+1] & Y_a[L] & \cdots & Y_a[1] \\ Y_a[L+2] & Y_a[L+1] & & Y_a[2] \\ \vdots & \vdots & \ddots & \\ Y_a[2L] & Y_a[2L-1] & \cdots & Y_a[L] \\ \vdots & \vdots & & \end{pmatrix} \begin{pmatrix} H[0] \\ H[1] \\ \vdots \\ H[L] \end{pmatrix} = 0. \tag{3.7}$$

Since $H(z)$ has multiple roots at $z_l = e^{-j\omega_0\tau_l}$, τ_l can be calculated as $\tau_l =$

$-j\frac{\ln(z_l)}{\omega_0}$. We can represent $h(t)$ in (2.2) as a FIR filter

$$h(t) = \sum_{m=0}^{M-1} a_m \delta(t - mT_h), \tag{3.8}$$

where $M \geq \frac{L\tau_L}{T_h}$ and T_h is the time delay between each filter tap. In this case, the unknown τ_l-spaced delta functions in (2.2) are replaced by T_h-spaced resolvable delta functions. In this case, $Y_a[n]$ can be represented as

$$Y_a[n] = \sum_{m=0}^{M-1} a_m e^{-j\Omega nm} + \eta[n], \tag{3.9}$$

where $\Omega = \frac{2\pi}{M}$ and $\eta(n) = \mathcal{N}(n)/S(n)$.

Expanding (3.9) we get

$$\begin{pmatrix} e^{-j\Omega(0)(0)} & e^{-j\Omega(0)(1)} & \dots & e^{-j\Omega(0)(M-1)} \\ e^{-j\Omega(1)(0)} & e^{-j\Omega(1)(1)} & & e^{-j\Omega(1)(M-1)} \\ \vdots & \vdots & \ddots & \\ e^{-j\Omega(M-1)(0)} & e^{-j\Omega(M-1)(1)} & \dots & e^{-j\Omega(M-1)(M-1)} \end{pmatrix} \begin{pmatrix} a[0] \\ a[1] \\ \vdots \\ a[M-1] \end{pmatrix} + \begin{pmatrix} \eta[0] \\ \eta[1] \\ \vdots \\ \eta[M-1] \end{pmatrix} = \begin{pmatrix} Y_a[0] \\ Y_a[1] \\ \vdots \\ Y_a[M-1] \end{pmatrix}. \tag{3.10}$$

For simplicity we represent (3.10) as

$$\widetilde{Y}_a = F\,\boldsymbol{a} + \boldsymbol{\eta}. \tag{3.11}$$

3.3 Low-Dimensional Signal Preliminaries

Signals can often be well-approximated as a linear combination of just a few elements from a known basis or dictionary. Sparse signal models provide a mathematical framework for capturing the fact that in many cases these high-dimensional signals contain relatively little information compared to their ambient dimension.

3.3.1 Sparsity and Nonlinear Approximation

Mathematically, we say that a signal $\boldsymbol{x}$ is k-sparse when it has at most k nonzeros, i.e., $\|\boldsymbol{x}\|_0 \leq k$, where $\|\boldsymbol{x}\|_0$ is the total number of non-zero elements in $\boldsymbol{x}$. In this case

$$\Sigma_k = \{\boldsymbol{x} : \|\boldsymbol{x}\|_0 \leq k\} \tag{3.12}$$

denote the set of all k-sparse signals, where ℓ_p-norm is denoted as $\|\boldsymbol{x}\|_p := \left(\sum_{n=0}^{N-1} |x_n|^p\right)^{\frac{1}{p}}$ where $p \geq 1$. Some signals are not sparse themselves, but they have a sparse representation in some basis Φ. In this case we will still refer to $\boldsymbol{x}$ as being k-sparse, with the understanding that we can express $\boldsymbol{x}$ as

$$\boldsymbol{x} = \Phi \boldsymbol{c}, \tag{3.13}$$

where $\|\boldsymbol{c}\|_0 \leq k$.

Sparsity has long been exploited in signal processing and approximation theory for tasks such as compression [35–39] and denoising [40, 41], and in statistics and learning theory as a method for avoiding over fitting [42–44]. Sparsity

also figures prominently in the theory of statistical estimation and model selection [45,46], in the study of the human visual system [47], and has been exploited heavily in image processing tasks [48, 49].

However, only a few real-world signals are truly sparse; the majority of the signals are compressible which means that they can be well-approximated by sparse signals. Such signals have been termed compressible, approximately sparse, or relatively sparse in various contexts. In fact, we can quantify the compressibility by calculating the error incurred by approximating a signal $\boldsymbol{x}$ by some $\widehat{\boldsymbol{x}} \in \Sigma_k$

$$\sigma_k(\boldsymbol{x})_p = \min_{\hat{x} \in \Sigma_k} \|\boldsymbol{x} - \widehat{\boldsymbol{x}}\|_p. \tag{3.14}$$

If $\boldsymbol{x} \in \Sigma_k$, then clearly $\sigma_k(\boldsymbol{x})_p = 0$ for any p. Moreover, we can show that the thresholding strategy described above (keeping only the k largest coefficients) results in the optimal approximation as measured by (3.14) for all ℓ_p norms [50].

Sparsity is a highly nonlinear model, since the choice of which dictionary elements are used can change from signal to signal [50]. This can be seen by observing that given a pair of k-sparse signals, a linear combination of the two signals will in general no longer be k-sparse, since their supports may not coincide. That is, for any $\boldsymbol{x}, \boldsymbol{z} \in \Sigma_k$, we do not necessarily have that $\boldsymbol{x} + \boldsymbol{z} \in \Sigma_k$ (although we do have that $\boldsymbol{x} + \boldsymbol{z} \in \Sigma_{2k}$).

3.4 UWB Compressive Sensing Preliminaries

When the short duration UWB pulses propagate through the multipath channel, the received signal remains sparse in time domain. UWB signals can take zeros

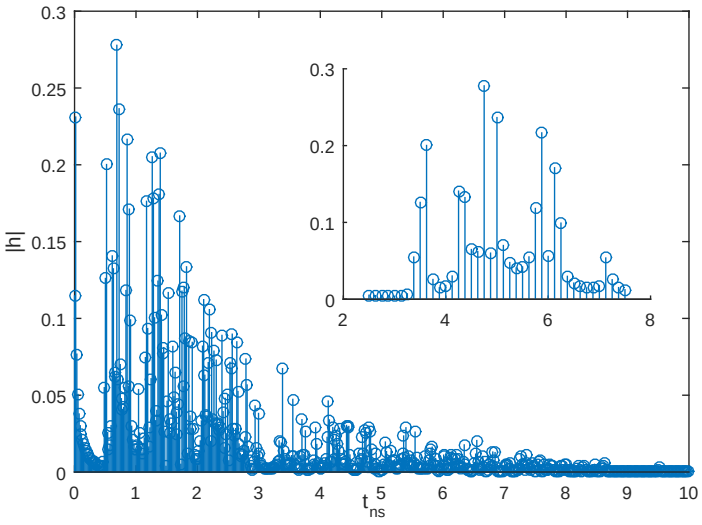

Figure 3.1: Sparcity in UWB channel impulse response.

or negligible values in a relatively long time interval, due to its nature in which the received signal is composed of separate clusters and spaced rays in each cluster. Therefore, it is obvious that the UWB channel is sparse/pseudo sparse [1]. A typical UWB CIR is depicted in Fig. 3.1. As it can be clearly seen the CIR takes negligible values in a relatively long time interval. More details about sparsity in UWB channels is investigated in [51, 52]. CS theory declares that in certain cases, when a signal is sparse, that is, if its information rate is lower than the Nyquist rate, the signal can be recovered from fewer samples than dictated by the Shannon-Nyquist theorem. Let $\boldsymbol{x} \in \mathbb{C}^N$ denotes the discrete-time signal which can be represented by some basis $\Psi \in \mathbb{C}^{N \times N}$ and the weighting coefficient

[1] We can call it pseudo sparse because there are negligible values rather than zeros.

$\boldsymbol{\theta} \in \mathbb{C}^N$ as

$$\boldsymbol{x} = \sum_{n=0}^{N-1} \psi_n \boldsymbol{\theta}_n = \Psi\boldsymbol{\theta}. \tag{3.15}$$

If $\boldsymbol{\theta}$ has only M non-zero coefficients, $M \ll N$, then $\boldsymbol{x}$ is an M-sparse signal and can be expressed as

$$\boldsymbol{x} = \sum_{i=0}^{M-1} \psi_{n_i} \boldsymbol{\theta}_{n_i} = \Psi\boldsymbol{\theta}, \tag{3.16}$$

where n_i denotes the index of the non-zero elements of $\boldsymbol{\theta}$. By projecting $\boldsymbol{x}$ onto a random measurement matrix, $\Phi \in \mathbb{C}^{K\times N}$, where $K \ll N$, a set of measurement $\boldsymbol{y} = \Phi\Psi\boldsymbol{\theta}$ can be obtained. In the absence of noise (ideal case), $\boldsymbol{\theta}$ can be estimated as

$$\boldsymbol{\theta} = \arg\min \|\boldsymbol{\theta}\|_1 \text{ subject to } \boldsymbol{y} = \Phi\Psi\boldsymbol{\theta}, \tag{3.17}$$

where ℓ_p-norm is denoted as $\|\boldsymbol{\theta}\|_p := \left(\sum_{n=0}^{N-1} |\theta_n|^p\right)^{\frac{1}{p}}$. However, in real scenarios, the measurement is corrupted by noise, $\boldsymbol{x} = \Psi\boldsymbol{\theta} + \boldsymbol{n}$. Therefore

$$\boldsymbol{y} = \Phi\Psi\boldsymbol{\theta} + \boldsymbol{z}, \tag{3.18}$$

where $\boldsymbol{z} = \Phi\boldsymbol{n}$. In this case, $\boldsymbol{\theta}$ can be estimated as

$$\boldsymbol{\theta} = \arg\min \|\boldsymbol{\theta}\|_1 \text{ subject to } \|\boldsymbol{y} - \Phi\Psi\boldsymbol{\theta}\|_2 \leq \epsilon, \tag{3.19}$$

where $\epsilon \geq \|\boldsymbol{z}\|_2$.

There are two main theoretical questions in CS. First, how should we design the sensing matrix $A \in \mathbb{C}^{m\times n}$ to ensure that it preserves the information in the signal $\boldsymbol{x}$? Second, how can we recover the original signal $\boldsymbol{x}$ from measurements

$\boldsymbol{y}$? When the data is sparse or compressible, matrix A can be designed to ensure that the original signal can be recovered accurately and efficiently by using a variety of practical algorithms.

While there exist a wide variety of approaches to recover the sparse signal $\boldsymbol{x}$, the first natural approach is to attempt to recover $\boldsymbol{x}$ by solving an optimization problem of the following form

$$\widehat{\boldsymbol{x}} = \underset{\boldsymbol{z}}{\operatorname{argmin}} \|\boldsymbol{z}\|_0 \text{ subject to } \boldsymbol{z} \in \mathcal{B}(\boldsymbol{y}), \tag{3.20}$$

where $\mathcal{B}(\boldsymbol{y})$ ensures that $\widehat{\boldsymbol{x}}$ is consistent with the measurements $\boldsymbol{y}$. In the case when the measurements are exact and noise-free, the following equation holds $\mathcal{B}(\boldsymbol{y}) = \{\boldsymbol{z} : A\boldsymbol{z} = \boldsymbol{y}\}$. When the measurements are contaminated by a small amount of bounded noise, we have

$$\mathcal{B}(\boldsymbol{y}) = \{\boldsymbol{z} : \|A\boldsymbol{z} - \boldsymbol{y}\|_2 \leq \epsilon\}. \tag{3.21}$$

In both cases, (3.20) finds the sparsest $\boldsymbol{x}$ that is consistent with the measurements $\boldsymbol{y}$. In (3.20) we are inherently assuming that $\boldsymbol{x}$ itself is sparse.

The more common setting is where $\boldsymbol{x} = \Phi\boldsymbol{c}$. In this case, the approach is modified and we instead consider

$$\widehat{\boldsymbol{c}} = \underset{\boldsymbol{z}}{\operatorname{argmin}} \|\boldsymbol{z}\|_0 \text{ subject to } \boldsymbol{z} \in \mathcal{B}(\boldsymbol{y}), \tag{3.22}$$

where $\mathcal{B}(\boldsymbol{y}) = \{\boldsymbol{z} : A\Phi\boldsymbol{z} = \boldsymbol{y}\}$ or $\mathcal{B}(\boldsymbol{y}) = \{\boldsymbol{z} : \|A\boldsymbol{z} - \boldsymbol{y}\|_2 \leq \epsilon\}$. By considering $\widetilde{A} = A\Phi$ we see that (3.20) and (3.22) are essentially identical. Moreover, in many cases the introduction of Φ does not significantly complicate the construc-

tion of matrix A such that $\widetilde{A}$ will satisfy the desired properties.

Since the objective function $\|.\|_0$ in (3.20) is nonconvex and hence potentially very difficult to solve, a more tractable approach is to replace $\|.\|_0$ with its convex approximation $\|.\|_1$. Specifically, we consider

$$\widehat{\boldsymbol{x}} = \underset{\boldsymbol{z}}{\operatorname{argmin}} \|\boldsymbol{z}\|_1 \text{ subject to } \boldsymbol{z} \in \mathcal{B}(\boldsymbol{y}). \tag{3.23}$$

Provided that $\mathcal{B}(\boldsymbol{y})$ is convex, (3.23) is computationally solvable. In fact, when $\mathcal{B}(\boldsymbol{y}) = \{\boldsymbol{x} : A\boldsymbol{z} = \boldsymbol{y}\}$, the resulting problem can be posed as a linear programming problem [53].

3.5 Coarse Graining for Compressive Sensing UWB Channel Estimation

We propose a CG technique for the CS-UWB channel estimation algorithm to further reduce the complexity of channel estimation and the sampling rate. First, a quick review of the mathematical expression for the CG technique is provided and then the effects of employing it in UWB channel estimation are investigated.

3.5.1 Coarse Graining Preliminaries

The term of CG can be used to refer to any technique (usually in molecular systems) that simplifies a system by grouping several atoms/nodes of it into one component, thus to consist of fewer, larger components. In a large complex network, CG can be used to reduce the number of nodes and edges by means of a

mapping of the network with N nodes and E edges into a smaller network with $\widetilde{N}$ nodes and $\widetilde{E}$ edges, where $\widetilde{N}$ and $\widetilde{E}$ must be small enough to be amenable to analysis and visualization.

Definition 1: A linear mapping in the form of LMR^* which transforms (maps) $M \in \mathbb{C}^{n\times n}$ to $\widetilde{M} \in \mathbb{C}^{m\times m}$ is a CG transformation if

1. $m \leq n$
2. $L, R \in \mathbb{C}^{m\times n}$ s.t. $LR^* = I_m$

where L and R are referred to as semi-projector matrices and $P = R^*L$ as a projection matrix of rank m [54].

3.5.2 Coarse Graining in UWB

The aim here is to reduce the complexity of UWB channel estimation by shrinking matrix F in (3.11) in order to estimate only a few element of $\boldsymbol{a}$. CG transformations can be applied in UWB channel estimation to decrease the sampling rate and decrease the number of samples because we are interested in estimating only the dominant components $\boldsymbol{a}$ not all components of $\boldsymbol{a}$. Let $F_s \in \mathbb{C}^{P\times P}$ represent a shrunk version of F which is related to $\boldsymbol{a}_s = [a_0, a_2, \ldots, a_{P-1}]^T$, where $P < N$ is the number of desirable paths to be estimated. In this case, $\Phi_s \in \mathbb{C}^{P\times P}$ is the new projection matrix corresponding to F_s and $\boldsymbol{a}_s \in \mathbb{C}^{P\times 1}$. A shrinking matrix $T = \left(I_P \;\middle|\; 0\right) \in \mathbb{R}^{P\times N}$ can be applied to Ψ as

$$F_s = T\,F\,T^*. \tag{3.24}$$

The shrunk version of $\Phi\ F_s \boldsymbol{a}_s$ is given by

$$\Phi_s F_s \boldsymbol{a}_s = \left(\Phi_s \;\middle|\; \Phi_B\right) T \left(\begin{array}{c|c} F_s & F_B \\ \hline F_C & F_D \end{array}\right) T^* \, \boldsymbol{a}_s. \tag{3.25}$$

From Definition 1, we can see that T can be used as a semi-projector for CG technique. In this case, $L = R = T$ and

$$P = \left(\begin{array}{c} I_P \\ \hline 0 \end{array}\right) \left(I_P \;\middle|\; 0\right) = \left(\begin{array}{c|c} I_P & 0 \\ \hline 0 & 0 \end{array}\right), \tag{3.26}$$

$$LR^* = \left(I_P \;\middle|\; 0\right) \left(\begin{array}{c} I_P \\ \hline 0 \end{array}\right) = I_P. \tag{3.27}$$

3.5.3 ℓ_1-Optimization for the Proposed Coarse Graining Technique in UWB Channel Estimation

In this section, a closed-form expression for ℓ_1-optimization for the proposed method is derived. By applying CG in (3.11), we have

$$\boldsymbol{a}_s = \arg\min_{a_s} \|a_s\|_1 \text{ subject to } \|\boldsymbol{\gamma}_s - \Phi_s F_s a_s\|_2 \leq \epsilon, \tag{3.28}$$

where $\boldsymbol{\gamma}_s = \Phi \Gamma_b$. Using the Lagrangian method, (3.28) can be rewritten as

$$\boldsymbol{a}_s = \arg\min_{a_s} \frac{1}{2} \|\boldsymbol{\gamma}_s - \Phi_s F_s \boldsymbol{a}_s\|_2^2 + \lambda \|\boldsymbol{a}_s\|_1, \tag{3.29}$$

where λ is the Lagrange multiplier and $\|\boldsymbol{a}_s\|_1 = \sum_i \left(x_i^2 + y_i^2\right)^{1/2}$ is ℓ_1 of the complex vector $\boldsymbol{a}_s$ in which x_i and y_i are real and imaginary parts of i-th element of $\boldsymbol{a}_s$, respectively [55]. To represent (3.29) as a quadratic programming with inequality constraints, we use the truncated Newton interior-point method (TNIPM) [56]. Therefore, (3.29) is recast as

$$\begin{aligned} \min_{x,y,u} \sum_i u_i \quad \text{subject to} \quad & f_{u,i}(x_i, y_i, u_i) \leq 0, \\ & f_\epsilon(x_i, y_i, u_i) \leq 0, \quad i = 1, 2, \cdots, P, \end{aligned} \tag{3.30}$$

where $f_{u,i}(x, y, u) = \sqrt{x_i^2 + y_i^2} - u_i$, $f_\epsilon(x, y, u) = \frac{1}{2}\left(\|\widetilde{\Phi_s F_s}\boldsymbol{a}_s - \boldsymbol{\gamma}_s\|_2^2 - \epsilon^2\right)$ and

$$\widetilde{\Phi_s F_s} = \begin{pmatrix} \mathrm{Re}\{\Phi_s F_s\} & -\mathrm{Im}\{\Phi_s F_s\} \\ \mathrm{Im}\{\Phi_s F_s\} & \mathrm{Re}\{\Phi_s F_s\} \end{pmatrix},$$

$$\boldsymbol{\gamma}_s = \begin{pmatrix} \mathrm{Re}\{\boldsymbol{\gamma}_s\} \\ \mathrm{Im}\{\boldsymbol{\gamma}_s\} \end{pmatrix},$$

$$\boldsymbol{a}_s = \begin{pmatrix} \mathrm{Re}\{\boldsymbol{a}_s\} \\ \mathrm{Im}\{\boldsymbol{a}_s\} \end{pmatrix}.$$

The standard log-barrier method is used to transform (3.30) into linearly constrained program. In this case, for the k-th iteration we have

$$\min_{x,y,u} f(x, y, u) = \min_{x,y,u} \sum_i u_i + \frac{1}{\tau^k}\Xi(x, y, u), \tag{3.31}$$

where τ increases as Newton iterations progress and

$$\Xi(x,y,u) = -\left(\sum_i \log\left(-f_{u,i}(x,y,u)\right) + \log\left(-f_\epsilon(x,y,u)\right)\right). \tag{3.32}$$

By expanding $f(x,y,u)$ around (x,y,u) according to Taylor's formula, we have

$$\begin{aligned} f(x+\Delta x, y+\Delta y, u+\Delta u) \approx\ & f(x,y,u) + \nabla f(x,y,u)\,(\Delta x,\Delta y,\Delta u)^T \\ & + \frac{1}{2}(\Delta x,\Delta y,\Delta u)\,\mathrm{H}f(x,y,u)\,(\Delta x,\Delta y,\Delta u)^T, \end{aligned} \tag{3.33}$$

where $\nabla f(x,y,u)$ and $\mathrm{H}f(x,y,u) = \mathbf{J}(\nabla f(x,y,u))$ are the gradient vector and Hessian matrix of $f(x,y,u)$, respectively, which can be calculated as [2]

$$\begin{aligned} \nabla f(x,y,u) = \frac{1}{\tau}\Bigg(& -f_u^{-1}\frac{x}{\sqrt{x^2+y^2}} - f_\epsilon^{-1}\boldsymbol{r}^T\widetilde{\Phi_s F_s}\left(\frac{\partial \boldsymbol{a}_s}{\partial x}\right), \\ & -f_u^{-1}\frac{y}{\sqrt{x^2+y^2}} - f_\epsilon^{-1}\boldsymbol{r}^T\widetilde{\Phi_s F_s}\left(\frac{\partial \boldsymbol{a}_s}{\partial y}\right), f_u^{-1}+\tau\Bigg), \end{aligned} \tag{3.34}$$

[2] $\mathbf{J}$ is the Jacobian matrix.

$$
\begin{aligned}
H_{11} &= \frac{1}{\tau}\left(-f_u^{-1}\frac{y^2}{(x^2+y^2)^{3/2}} + f_u^{-2}\frac{x^2}{x^2+y^2} - f_\epsilon^{-1}\left(\frac{\partial \boldsymbol{a}_s}{\partial x}\right)^T \widetilde{\Phi_s F_s}^T \widetilde{\Phi_s \boldsymbol{F}_s}\left(\frac{\partial \boldsymbol{a}_s}{\partial x}\right)\right.\\
&\quad \left. + f_\epsilon^{-2}\boldsymbol{r}^T\widetilde{\Phi_s F_s}\left(\frac{\partial \boldsymbol{a}_s}{\partial x}\right)\left(\frac{\partial \boldsymbol{a}_s}{\partial x}\right)^T \widetilde{\Phi_s F_s}^T \boldsymbol{r}\right),\\
H_{12} &= \frac{1}{\tau}\left(f_u^{-2}\frac{xy}{x^2+y^2} - f_u^{-1}\frac{xy}{(x^2+y^2)^{3/2}} - f_\epsilon^{-1}\left(\frac{\partial \boldsymbol{a}_s}{\partial x}\right)^T \widetilde{\Phi_s F_s}^T \widetilde{\Phi_s F_s}\left(\frac{\partial \boldsymbol{a}_s}{\partial y}\right)\right.\\
&\quad \left. + f_\epsilon^{-2}\boldsymbol{r}^T\widetilde{\Phi_s F_s}\left(\frac{\partial \boldsymbol{a}_s}{\partial y}\right)\left(\frac{\partial \boldsymbol{a}_s}{\partial x}\right)^T {\Phi_s F_s}^T \boldsymbol{r}\right),\\
H_{13} &= H_{31} = -\frac{1}{\tau}\left(f_u^{-2}\frac{x}{\sqrt{x^2+y^2}}\right),\\
H_{21} &= \frac{1}{\tau}\left(f_u^{-2}\frac{xy}{x^2+y^2} - f_u^{-1}\frac{xy}{(x^2+y^2)^{3/2}} - f_\epsilon^{-1}\left(\frac{\partial \boldsymbol{a}_s}{\partial y}\right)^T \widetilde{\Phi_s F_s}^T \widetilde{\Phi_s F_s}\left(\frac{\partial \boldsymbol{a}_s}{\partial x}\right)\right.\\
&\quad \left. + f_\epsilon^{-2}\boldsymbol{r}^T\widetilde{\Phi_s F_s}\left(\frac{\partial \boldsymbol{a}_s}{\partial x}\right)\left(\frac{\partial \boldsymbol{a}_s}{\partial y}\right)^T \widetilde{\Phi_s F_s}^T \boldsymbol{r}\right),\\
H_{22} &= \frac{1}{\tau}\left(-f_u^{-1}\frac{x^2}{(x^2+y^2)^{3/2}} + f_u^{-2}\frac{y^2}{x^2+y^2} - f_\epsilon^{-1}\left(\frac{\partial \boldsymbol{a}_s}{\partial y}\right)^T \widetilde{\Phi_s F_s}^T \widetilde{\Phi_s F_s}\left(\frac{\partial \boldsymbol{a}_s}{\partial y}\right)\right.\\
&\quad \left. + f_\epsilon^{-2}\boldsymbol{r}^T\widetilde{\Phi_s F_s}\left(\frac{\partial \boldsymbol{a}_s}{\partial y}\right)\left(\frac{\partial \boldsymbol{a}_s}{\partial y}\right)^T \widetilde{\Phi_s F_s}^T \boldsymbol{r}\right),\\
H_{23} &= H_{32} = -\frac{1}{\tau}\left(f_u^{-2}\frac{y}{\sqrt{x^2+y^2}}\right),\\
H_{33} &= \frac{1}{\tau}f_u^{-2};
\end{aligned}
\tag{3.35}
$$

where $\boldsymbol{r} = \widetilde{\Phi_s F_s}\boldsymbol{a}_s - \widetilde{\gamma}_s$,

$$
\frac{\partial \boldsymbol{a}_s}{\partial x} = \left(\begin{array}{c|c} I_P & 0 \\ \hline 0 & 0 \end{array}\right), \tag{3.36}
$$

Table 3.1: Innovation rates for LOS/NLOS UWB channels

LOS	NLOS
0.0265	0.0535

and

$$\frac{\partial \boldsymbol{a}_s}{\partial y} = \left(\begin{array}{c|c} 0 & 0 \\ \hline 0 & I_P \end{array}\right). \tag{3.37}$$

Finally, the Newton's step in the log-barrier method which minimizes $f\left(x+\Delta x, y+\Delta y, u+\Delta u\right)$ is given by

$$\left(\Delta x, \Delta y, \Delta u\right)^T = -H^{-1} f\left(x, y, u\right) \nabla^T f\left(x, y, u\right). \tag{3.38}$$

3.6 Performance Results and Discussion

In this section we validate the performance of the proposed method. Simulations are performed particularly for the indoor office LOS channel and indoor office NLOS channel proposed by the IEEE 802.15.4a Task Group. We validate the innovation rate of UWB CIR based on (3.2) for indoor LOS/NLOS environments. If we assume that the UWB signal is periodic, then (3.2) is valid for UWB signals/channels and provides an innovation rate comparison among indoor LOS/NLOS channels/signals. The experimental innovation rates for the LOS/NLOS channels are summarized in Table 3.1. It is clear that the innovation rate for the indoor NLOS environments is much greater than indoor LOS environments. CIR amplitude root mean squared error (RMSE) performance of the proposed method is also investigated for different scenarios in this section.

To have a fair comparison between LOS and NLOS channel environments in CS method, we develop scenarios in which the ratio of the number of measurement M to the total possible measurement N, $r = \frac{M}{N}$ is fixed. Also, to investigate the effects of the proposed CG algorithm in CS channel estimation, we suppose the difference between the number of interested paths P and the total possible measurement N, is fixed $d = N - P$. As it is clearly seen in Fig. 3.2, when neither CS nor CG techniques is applied on channel estimation/synchronization, the RMSE is significantly lower compared with other cases, because in this case, none of the measurement has been discarded. Also, it can be seen that when we increase the number of measurement from $r = 30\%$ to $r = 50\%$, the RMSE performance improves, because we consider more measurement/information in channel estimation in this case. In Fig. 3.3, CIR amplitude RMSE is shown as a function of SNR for the proposed CG schemes. As it is depicted, when the CG algorithm is applied, for small d, the performance is still close to that of the scenarios when only CS is applied for channel estimation and synchronization. As d increases, the number of discarded paths increases and consequently the RMSE increases. By applying CG in CS UWB channel estimation, we decrease the computational complexity by estimating only main components (first dominant components) while the benefits of CS are still retained, i.e., decreased sampling rate.

3.7 Conclusion

We have proposed a CG technique in CS theory to lower the computational complexity and to decrease the required sampling rate in UWB channel estimation.

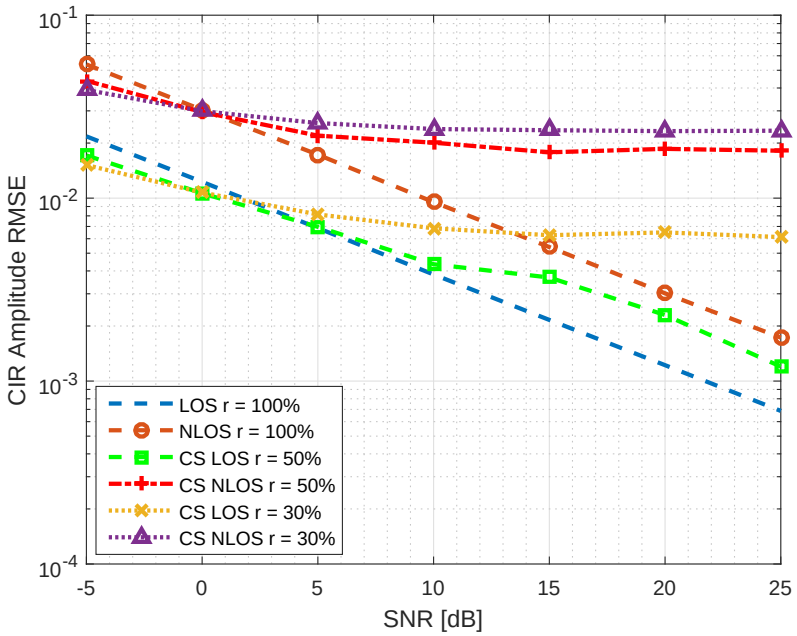

Figure 3.2: CIR amplitude RMSE in LOS/NLOS environments with proposed CS CIR estimation method.

In the proposed method, by smoothing away non-dominant components in the received signal via the CG technique, we only estimate the dominant paths which typically capture more than 70% of the total received energy. The innovation rates of different UWB channels were investigated for UWB LOS/NLOS environments. Results showed that NLOS channels have higher innovation rates (degree of freedom) and simulation results illustrated the performance of the proposed algorithm in different channel environments.

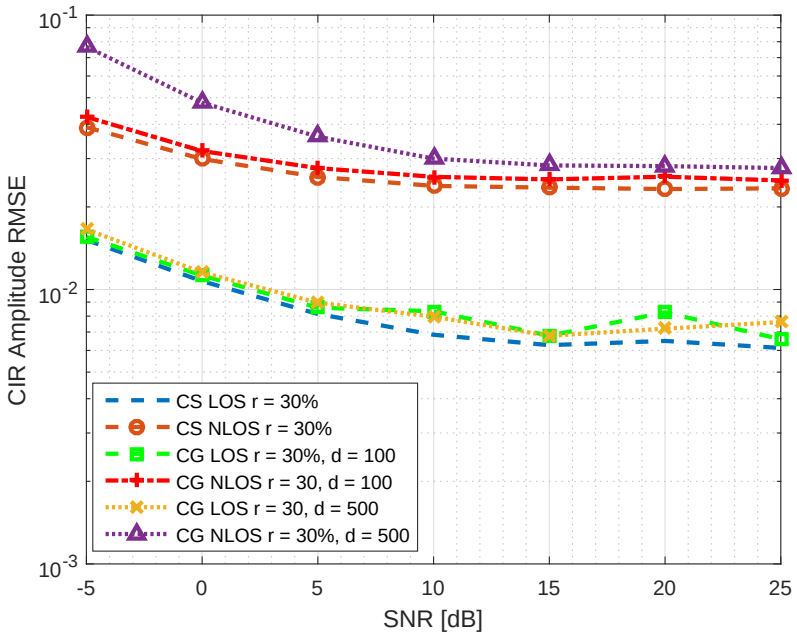

Figure 3.3: CIR amplitude RMSE in LOS/NLOS environments with the proposed CG algorithm in CS CIR estimation.

Chapter 4 – UWB Channel Calssification

4.1 Introduction

Classification of LOS or NLOS propagation is critical for most pulsed ultrawideband localization systems. In this chapter, first, we propose a 2-dimensional (2-D) LOS/NLOS classification scheme that uses skewness of the channel impulse/pulse response, which has not been used by existing work.

Extensive work has studied NLOS propagation effects on UWB localization [57–72]. These efforts mainly address two areas: techniques to classify LOS/NLOS conditions [57, 58] and methods to mitigate the effects of NLOS [59, 60].

LOS/NLOS classification commonly uses the statistical parameters of the CIR or CPR [61–64], or range estimation [65]. For example, kurtosis, root mean square (RMS) delay spread, and mean excess delay are used in [61, 62]; cumulative distribution function (CDF) of the CPR along with kurtosis is used in [63]; rms delay spread, kurtosis, and maximum amplitude of the received signal are used in [64]. The time-of-arrival (TOA) error models for LOS/NLOS channels [65] can also be used for channel classification.

While extensive work in this area exists, one channel statistical parameter which has not been used in existing work is the skewness of the CIR or CPR. Skewness is a measure of symmetry, or more precisely, the lack of symmetry in the probability density function (PDF). A distribution, or data set, is symmetric

if it looks the same to the left and right of the center point; i.e., if the bulk of the data is at the left and the right tail is longer, then the distribution is skewed right, or positively skewed; if the peak is toward the right and the left tail is longer, then it is said the distribution is skewed left, or negatively skewed [73]. Since skewness characterizes the amount and direction of skew (departure from horizontal symmetry), it could be an effective parameter for LOS/NLOS classification; if the skewness of the impulse response of a UWB channel is high, then the channel is more likely to be LOS. We propose a 2-dimensional (2-D) LOS/NLOS classification scheme that uses skewness and demonstrate its effectiveness. This approach is much simpler than existing 3-D methods.

4.2 Statistical Channel Parameters Used in LOS/NLOS Classification

Channel statistical parameters which have been used in existing work for LOS/NLOS classification include:

- Kurtosis (k): The kurtosis of $|h(t)|$ is defined as $k = \frac{E[(|h(t)|-\mu_{|h|})^4]}{[E(|h(t)|-\mu_{|h|})^2]^2} = \frac{E[(|h(t)|-\mu_{|h|})^4]}{\sigma_{|h|}^4}$, where $\mu_{|h|}$ and $\sigma_{|h|}$ are the mean and standard deviation of $|h(t)|$, respectively [75];
- Mean excess delay (τ_m) [76];
- rms delay spread (τ_{rms}) [76].

4.2.1 Statistical Approach for Channel Classification

NLOS classification can be modeled as a binary hypothesis test. Let hypothesis H_0 denote LOS and H_1 denote NLOS. One approach is to make a binary decision based on a measured channel profile. Given the transmitted signal $s(t)$, the received signal is expressed as $r(t) = \sum_{l=0}^{L-1} \alpha_l s(t - \tau_l) + n(t)$.

The maximum likelihood (ML) hypothesis test is written as

$$f_{\boldsymbol{r}|H_0}(\boldsymbol{r}|H_0) \underset{H_1}{\overset{H_0}{\gtrless}} f_{\boldsymbol{r}|H_1}(\boldsymbol{r}|H_1), \tag{4.1}$$

where $\boldsymbol{r}$ is the vector representation of signal $r(t)$ in the Hilbert space, which is spanned by a complete orthonormal set of basis functions.

The conditional PDF is evaluated as [77]

$$\begin{aligned} f_{\boldsymbol{r}|H_i}(\boldsymbol{r}|H_i) &= \int \cdots \int f_{\boldsymbol{r}\boldsymbol{\theta}|H_i}(\boldsymbol{r}, \boldsymbol{\theta}|H_i) d\boldsymbol{\theta} \\ &= \int \cdots \int f_{\boldsymbol{r}|\boldsymbol{\theta},H_i}(\boldsymbol{r}|\boldsymbol{\theta}, H_i) f_{\boldsymbol{\theta}|H_i}(\boldsymbol{r}, \boldsymbol{\theta}|H_i) d\boldsymbol{\theta}, \qquad i = 0, 1 \end{aligned} \tag{4.2}$$

where $\boldsymbol{\theta}$ represents a vector of channel parameters such as path gains and delays. Evaluation of the multidimensional integration in (4.2) is computationally extensive. One way to resolve this problem is to treat $\boldsymbol{\theta}$ as if its statistics were unknown, resulting in a composite hypothesis test. A common approach to solve the composite hypothesis test is to estimate $\boldsymbol{\theta}$ under the assumptions H_0 and H_1, and use it as if $\boldsymbol{\theta}$ were known. In this case, the decision rule is given by

$$f_{\boldsymbol{r}|\boldsymbol{\theta}H_0}(\boldsymbol{r}|\hat{\boldsymbol{\theta}}_0, H_0) \underset{H_1}{\overset{H_0}{\gtrless}} f_{\boldsymbol{r}|\boldsymbol{\theta}H_1}(\boldsymbol{r}|\hat{\boldsymbol{\theta}}_1, H_1), \tag{4.3}$$

where $\hat{\boldsymbol{\theta}}_i$ denotes the estimate of $\boldsymbol{\theta}$ under hypothesis H_i. If a ML estimate of $\boldsymbol{\theta}$ is obtained, the hypothesis test becomes [77]

$$\max_{\boldsymbol{\theta}} f_{\boldsymbol{r}|\boldsymbol{\theta}H_0}(\boldsymbol{r}|\boldsymbol{\theta}, H_0) \underset{H_1}{\overset{H_0}{\gtrless}} \max_{\boldsymbol{\theta}} f_{\boldsymbol{r}|\boldsymbol{\theta}H_1}(\boldsymbol{r}|\boldsymbol{\theta}, H_1). \tag{4.4}$$

The likelihood ratio (LR) test can be performed for LOS/NLOS classification if some statistical information of the multipath channel is available. Kurtosis (k), the mean excess delay (τ_m), and the rms delay spread (τ_{rms}) can be used to capture the amplitude and delay statistics for the LOS and NLOS classification scenarios. If *a priori* knowledge of the statistics of k, τ_m, and τ_{rms} are available under LOS and NLOS scenarios in a certain environment, then a LR test can be performed for the hypothesis test.

4.3 Using Skewness in Channel Identification

For a certain channel realization $h(t)$, skewness of $|h(t)|$ is defined as

$$s = \frac{E[(|h(t)| - \mu_{|h|})^3]}{[E(|h(t)| - \mu_{|h|})^2]^{\frac{3}{2}}} = \frac{\mu^3}{\sigma^3}, \tag{4.5}$$

where μ^3 is the 3rd central moment of $|h(t)|$ [73].

The main contributions of this paper are as follows:

1. Developing a 2-D LR test that uses skewness;

2. Deriving a new method for assigning weights in the weighted least-square (WLS) algorithm based on the LR test;

3. Incorporating NLOS bias as a result of NLOS calcification for improved

localization.

4.3.1 Two Dimensional LR Test

Skewness can be added to parameters k, τ_m, and τ_{rms} that have been used by existing schemes as explained in Sec. 4.2.1. With skewness in the LR test, a suboptimal approach is to assume that all these parameters are independent. Thus the joint PDF is expressed as

$$\begin{aligned} f_{\boldsymbol{\theta}|H_0}(\boldsymbol{\theta}|H_0) &= f_{k|H_0}(k|H_0) \times f_{\tau_{rms}|H_0}(\tau_{rms}|H_0) \times f_{\tau_m|H_0}(\tau_m|H_0) \times f_{s|H_0}(s|H_0) \\ f_{\boldsymbol{\theta}|H_1}(\boldsymbol{\theta}|H_1) &= f_{k|H_1}(k|H_1) \times f_{\tau_{rms}|H_1}(\tau_{rms}|H_1) \times f_{\tau_m|H_1}(\tau_m|H_1) \times f_{s|H_1}(s|H_1), \end{aligned} \tag{4.6}$$

where $f_{k|H_0}(k|H_0)$, $f_{k|H_1}(k|H_1)$, $f_{\tau_m|H_0}(\tau_m|H_0)$, $f_{\tau_m|H_1}(\tau_m|H_1)$, $f_{\tau_{rms}|H_0}(\tau_{rms}|H_0)$, $f_{\tau_{rms}|H_1}(\tau_{rms}|H_1)$, $f_{s|H_0}(s|H_0)$ and $f_{s|H_1}(s|H_1)$ are the PDFs of the k, τ_m, τ_{rms}, and skewness for LOS and NLOS cases, respectively. The 4-D LR test becomes

$$K(\tau_{rms}, \tau_m, k, s) = \frac{f_{\boldsymbol{\theta}|H_0}(\boldsymbol{\theta}|H_0)}{f_{\boldsymbol{\theta}|H_1}(\boldsymbol{\theta}|H_1)}. \tag{4.7}$$

This 4-D LR test is complex and computationally intensive. A scheme that uses skewness and τ_{rms}, forming a 2-D test, is developed in this section. In this case, the suboptimal joint PDFs for LOS/NLOS classification becomes

$$\begin{aligned} f_{\boldsymbol{\theta}|H_0}(\boldsymbol{\theta}|H_0) &= f_{\tau_{rms}|H_0}(\tau_{rms}|H_0) \times f_{s|H_0}(s|H_0) \\ f_{\boldsymbol{\theta}|H_1}(\boldsymbol{\theta}|H_1) &= f_{\tau_{rms}|H_1}(\tau_{rms}|H_1) \times f_{s|H_1}(s|H_1). \end{aligned} \tag{4.8}$$

Table 4.1: Probability of uncertainty region

Method	sr	kre
Probability	0.0326	0.0500

Accordingly, the LR test is expressed as

$$K(\tau_{rms}, s) = \frac{f_{\boldsymbol{\theta}|H_0}(\boldsymbol{\theta}|H_0)}{f_{\boldsymbol{\theta}|H_1}(\boldsymbol{\theta}|H_1)}. \tag{4.9}$$

4.4 Simulation Results

This section presents results from simulation that uses the IEEE 802.15.4a channel model and experiments conducted in a realistic environment. Two channel models, indoor office LOS environment (CM3) and indoor office NLOS environment (CM4) [81], are considered. For simplicity, the various evaluated methods are called as:

1) kre: the method in [61], in which k, τ_m, and τ_{rms} are utilized in channel classification;

2) sr: the 2-D LOS/NLOS classification method proposed in this paper;

The uncertainty region in channel classification for different methods is depicted in Fig. 4.1. The exact values of the probability of falling in the uncertainty region with these two methods is summarized in Table 4.1; it is found that the proposed 2-D "sr" method reduces the probability of falling into the uncertainty region by about 35% compared to the 3-D "kre" method. These results show that skewness is an effective statistical parameter for channel classification. The

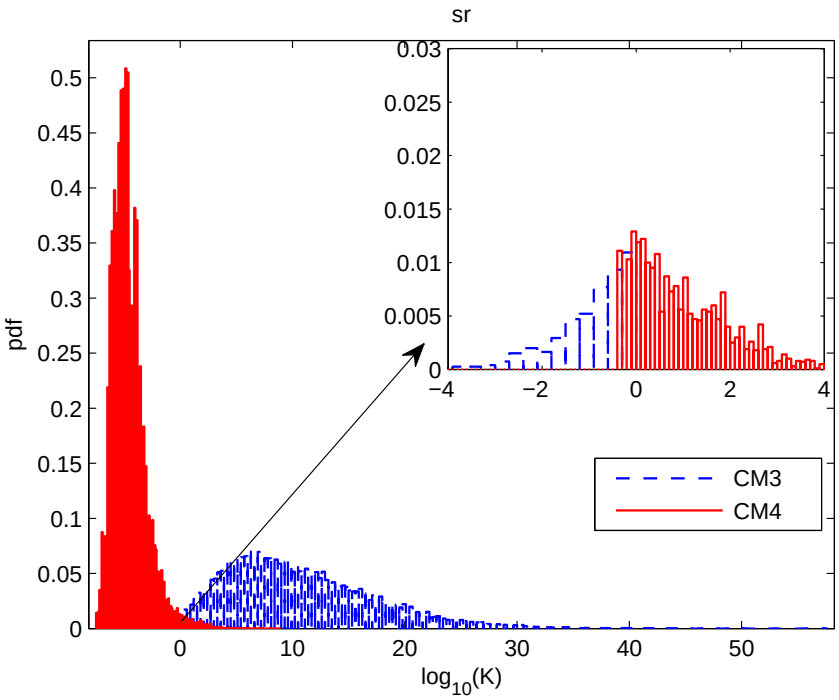

(a) PDF of $\log_{10} K(\tau_{rms}, s)$

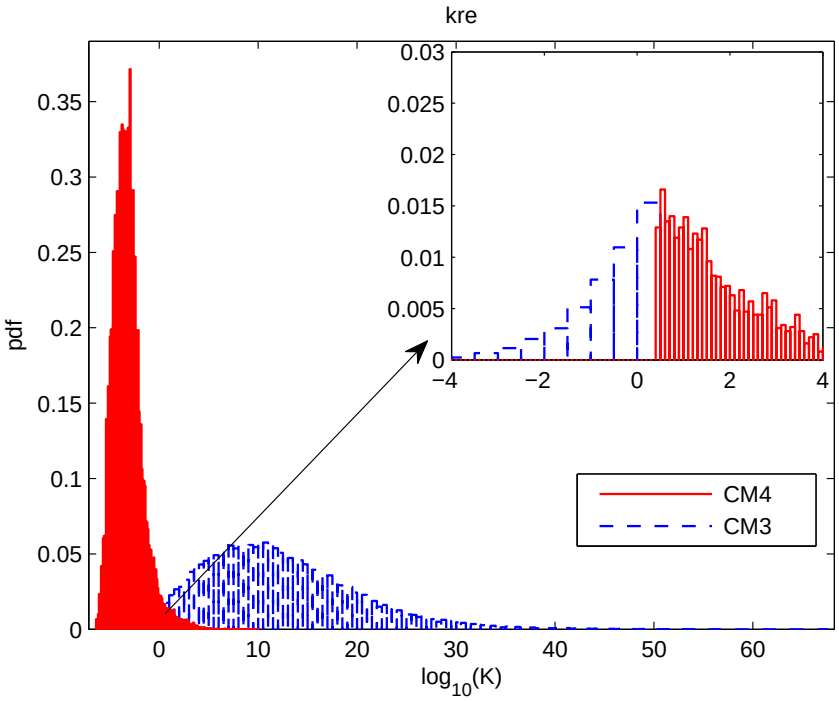

(b) PDF of $\log_{10} K(\tau_{rms}, \tau_m, k)$

Figure 4.1: PDF of the logarithm of the likelihood metric K for CM3 and CM4.

performances of various methods are also compared in terms of two following metrics [82]:

a) Probability of false alarm, P_{FA}: The probability that a LOS channel is declared (i.e., H0 is chosen) when the channel is in fact NLOS.

b) Probability of detection, P_D: The probability that the channel is classified as LOS (i.e., H0 is chosen) when the channel is in fact LOS.

P_{FA} is calculated as

$$P_{FA} = \int_{T}^{+\infty} f_{\boldsymbol{\theta}|H_1}(\boldsymbol{\theta}|H_1)\, d\theta, \tag{4.10}$$

where $f_{\boldsymbol{\theta}|H_1}(\boldsymbol{\theta}|H_1)$ is given by (4.6). Since the distributions of τ_{rms}, τ_m, k, and skewness are modeled as log-normal, $\boldsymbol{\theta}$ has also log-normal distribution. Thus

$$\begin{aligned} P_{FA} &= \int_{T}^{+\infty} \frac{1}{\sqrt{2\pi}\sigma_{H1}} e^{-\frac{(\theta-\mu_{H1})^2}{2\sigma_{H1}^2}} d\theta \\ &= \frac{1}{2}\left(1-\mathrm{erf}\left(\frac{T-\mu_{H1}}{\sqrt{2}\sigma_{H1}}\right)\right), \end{aligned} \tag{4.11}$$

where $\mathrm{erf}(x) = \frac{2}{\sqrt{\pi}} \int_0^x e^{-t^2} dt$.

The channel detection threshold, T, can be calculated for the specific P_{FA} in terms of the error function inverse as

$$T = \sqrt{2}\sigma_{H1}\mathrm{erf}^{-1}(1-2P_{FA}) + \mu_{H1}, \tag{4.12}$$

where μ_{H1} and σ_{H1} are the mean and standard deviation of the $\boldsymbol{\theta}$ in H1.

P_D is calculated as

$$\begin{aligned} P_D =& \int_T^{+\infty} f_{\boldsymbol{\theta}|H_0}(\boldsymbol{\theta}|H_0)\, d\theta = \int_T^{+\infty} \frac{1}{\sqrt{2\pi}\sigma_{H0}} e^{-\frac{(\theta-\mu_{H0})^2}{2\sigma_{H0}^2}} d\theta \\ =& \frac{1}{2}\left(1-\text{erf}\left(\frac{T-\mu_{H0}}{\sqrt{2}\sigma_{H0}}\right)\right). \end{aligned} \tag{4.13}$$

In the simulation, (μ_{H0}, μ_{H1}, σ_{H0}, σ_{H1}) for 3-D LR test "kre" and 2-D LR test "sr" methods are chosen as $(12.1238, -3.22323, 7.58917, 1.52168)$ and $(10.6321, -4.36144, 6.76482, 1.54776)$, respectively. Probability of detection P_D versus probability of false alarm P_{FA} is depicted in Fig. 4.2. It is observed that the proposed 2-D "sr" method has better performance in channel detection than the existing 3-D "kre" method. Since the "kre" method requires extracting three

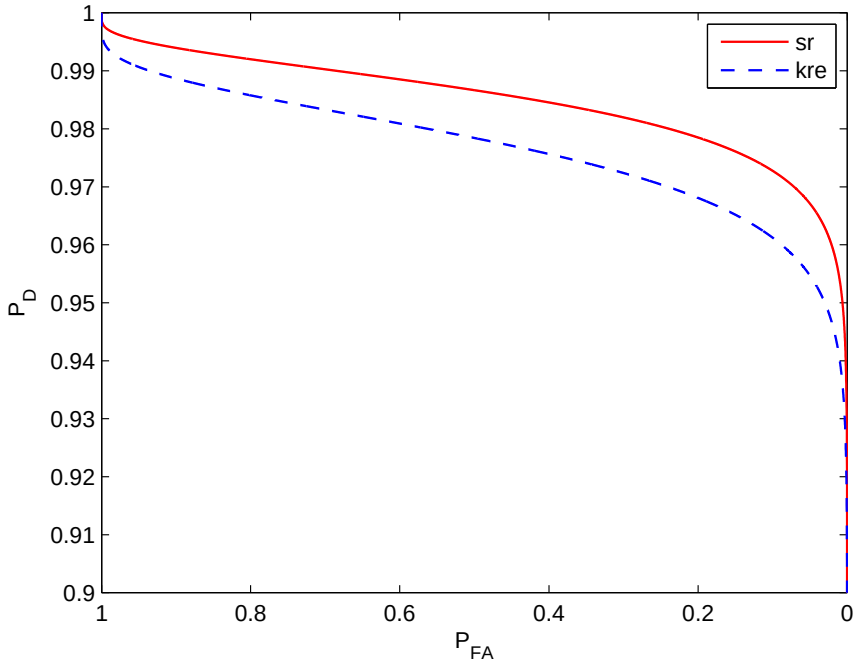

Figure 4.2: Probability of detection vs probability of false alarm.

statistical parameters of the channel while the proposed method requires only two, the proposed method is much simpler. The computational complexity of the proposed 2-D method is also lower than that of the 3-D method, since only two statistical parameters, rather than three, of the channel are needed for LR test.

4.4.1 Experimental Results

We have conducted extensive amount of experiments to verify the effectiveness of skewness for LOS/NLOS classification.

4.4.1.1 Experimental Environment and Setup

The experiment took place in a vacant building with an approximate dimension of $76m \times 40m \times 7m$. There are some small metal poles inside this space, but the propagation will be LOS unless a transmitter-receiver path is blocked intentionally. NLOS propagation scenarios in the experiment are created in two different ways: (1) a person stands in front of the receiver and blocks the direct path; and (2) a metal object is placed right in front of the receiver to block the direct path.

A pulsed UWB transmitter operating in the 3.1-5.1 GHz frequency range is used as the transmitter. The transmitted signals under LOS and NLOS conditions are received by a set of antennas optimized for operation in this frequency range and then filtered and amplified, which is then sampled by a real-time sampling scope operating at 12.5 Gsps. The sampled data are transferred to a PC

through Ethernet for further processing.

4.4.1.2 Results

Since the transmitted pulse shape is known and the pulse duration is very short (less than 1 ns), instead of obtaining the statistical channel parameters such as k, s, τ_m, and τ_{rms} from the CIR, which can be done, a simpler but still effective and accurate method is to obtain these parameters directly from the CPR as in some existing work [61–64]. LOS/NLOS classification results obtained by using 3-D method (k, τ_m, and τ_{rms}) and the proposed 2-D LR method (s and τ_{rms}) are shown in Fig. 4.3(a) and Fig. 4.3(b), respectively. The classification uncertainty region with the proposed 2-D LR test is 18% less than that with the 3-D LR test, demonstrating the effectiveness of using the skewness of the channel for LOS/NLOS classification. Note that the experimental environment does not fit exactly CM3 or CM4. Thus the difference between the simulation results in Fig. 1 and experimental results in Fig. 4 is expected. Nevertheless, the experimental results also verified the effectiveness of channel skewness for LOS/NLOS classification.

4.5 Conclusion

We have developed a LOS/NLOS channel classification scheme that uses skewness and rms delay spread of the CIR/CPR, and demonstrated its effectiveness. Compared with an existing 3-D classification scheme that requires obtaining three channel parameters, kurtosis, rms delay spread, and mean excess delay,

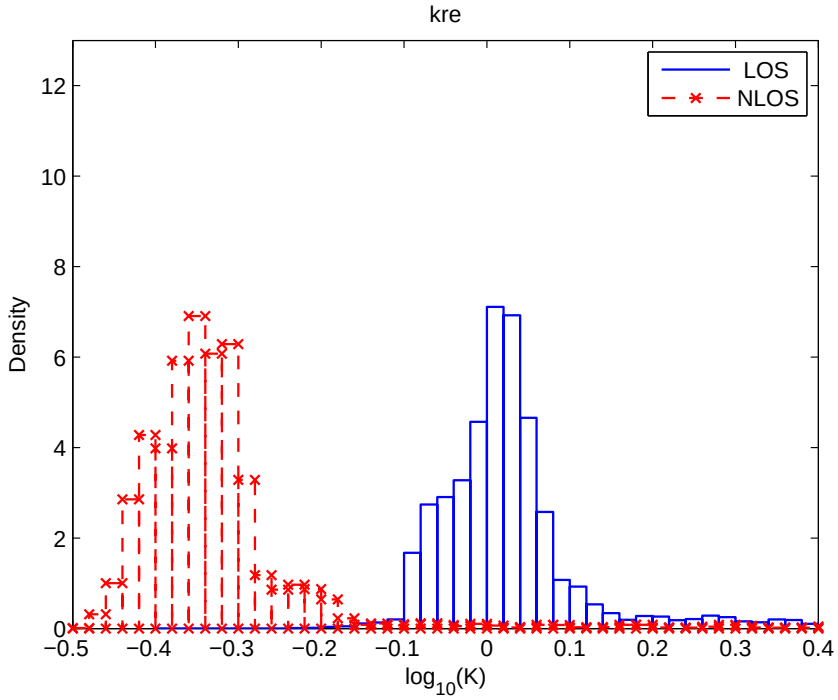

(a) PDF of $\log_{10} K(\tau_{rms}, \tau_m, k)$

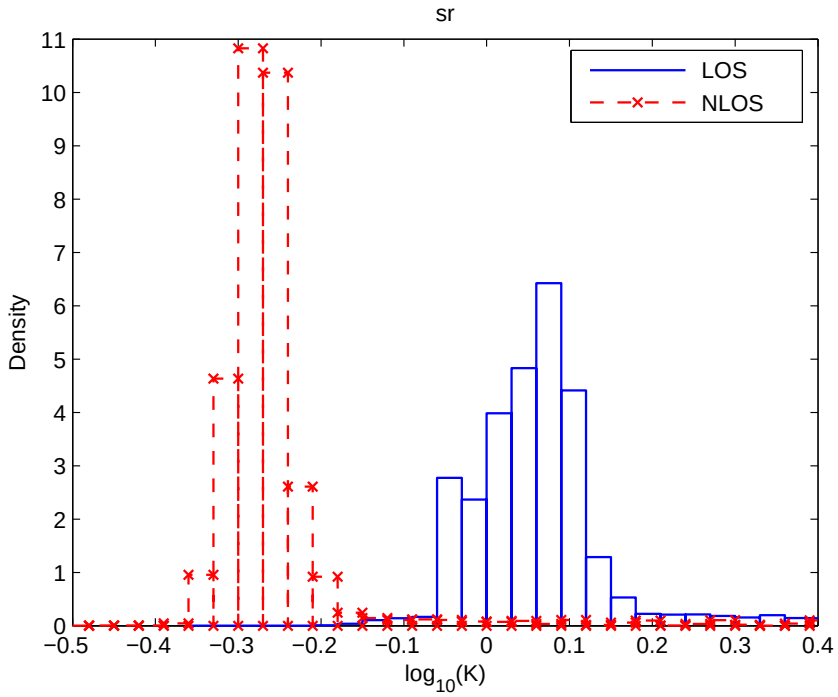

(b) PDF of $\log_{10} K(\tau_{rms}, s)$

Figure 4.3: PDF of the logarithm of the likelihood metric K from experimental data.

the proposed 2-D scheme is simpler. The proposed 2-D scheme also has a smaller classification ambiguity region than the 3-D scheme; in a typical indoor channel, the probability of falling into the uncertainty region of channel classification is reduced by about 35% with the proposed scheme when IEEE 802.15.4a channel models are assumed. In experiments conducted in a large vacant building, we observed an 18% reduction in the classification uncertainty region with the proposed 2-D method over a 3-D method.

Chapter 5 – UWB Relay Communications

5.1 Introduction

IR-UWB signaling is a promising technique for high-speed, short-range relay communications networks. Depending on how the relay node retransmits the signal, there are two main relay schemes: (1) conventional one-directional (one-way) relay model [83–88], and (2) bi-directional (two-way) relay model [89–91]. In bi-directional relay communications, wireless network coding (WNC), also known as physical-layer network coding (PNC), could be applied to overcome the spectral efficiency limitation of the conventional one-way relay schemes [83–91].

However, the current literature has mainly focused on the conventional synchronous links between the relay node (RN) and end nodes (ENs) [88–90]. The nature of the UWB signals require sub-nanosecond accurate timing synchronization which even after long acquisition signaling, there may still be some unknown residual timing offsets. To our knowledge, the effects of either the lack of synchronization or poor synchronization in the UWB relay communication systems have not been studied in the literature. In [88], perfect synchronization between RN and ENs links is assumed in analyzing the effects of multiuser interference (MUI) on the cooperative one-way amplify and forward (AF) and decode and forward (DF) relay schemes. Also, existing work has mainly focused on coherent modulation schemes which pose formidable challenges in system implementation [87–89]. To avoid the coherent demodulation challenges, transmit-

ted reference pulse (TRP) techniques [84, 85, 90] and differential demodulation schemes [83, 85, 86] have been proposed. However, all these schemes still require perfect time synchronization between RN and ENs even though they do not need channel state information (CSI) at the relay node. A coherent UWB symbol-by-symbol cooperation relay strategy that takes the orthogonal pulse position modulation (PPM) into consideration is proposed in [87]. An analytical model to study TH UWB relay communications is proposed in [88] which considers the effects of MUI in the UWB relay. In [90], a transmitted reference pulse cluster (TRPC) technique is proposed in PNC cooperative denoise and forward (DNF) relay strategy to avoid the need for coherent modulation. In [86], differential decoding one-way AF is presented where a new joint power allocation and path selection (JPAPS) scheme is proposed.

In this chapter, we propose and develop asynchronous, differential, and bidirectional decode and forward (ADBDF) and asynchronous, differential, and bidirectional denoise and forward (ADBDNF) UWB relay methods, where the relay does not need to be synchronized with the ENs. The proposed schemes are attractive for UWB communications for which stringent synchronization between the RN and the ENs may not be affordable for low-complexity UWB networks.

The rest of this chapter is organized as follows: differential detection technique used in the proposed schemes is reviewed in Sec. 5.2. In Sec. 5.3, we explain the advantages of employing relay in UWB communications. Sec. 5.4 presents the proposed ADBDF relay algorithm. In Sec. 5.5, the ADBDNF relay method will be explained. The performance achievable with the proposed relay communications schemes is investigated in Sec. 5.6

5.2 Bidirectional Relay Communications

Bidirectional (two-way) relay schemes have gained increasing attention in wireless communications as they are able to mitigate the inherent spectral loss of unidirectional protocols [92–94]. In half-duplex relay schemes two time phases are required to deliver only one unit of information, which loses half of the spectral efficiency [92]. Bidirectional relay systems are thus proposed to fully recover the rate loss, as only 2 time phases, i.e., broadcasting (BC) phase and multiple access (MA) phase, are required to accomplish the communication on both directions. Early work on bidirectional AF and bidirectional DF can be found in [92], which have shown significant improvements on sum-rates. Later, a new DNF protocol is proposed in [95], and a similar scheme called PNC is proposed in [96], where the condition to guarantee one-to-one mapping is also given. Later work in [97] shows that bidirectional DNF has higher sum-rates than bidirectional AF and bidirectional DF, and in [98] the closed-form BER of bidirectional DNF with coherent BPSK modulation in derived.

5.2.1 Decode and Forward

In DF relay schemes, the RN decodes the incoming signal from the ENs, and then re-encodes it prior to forwarding it to the destination [12]. In bidirectional DF, after decoding d_{AC} and d_{CA}, the RN B applies a canonical network coding operation and broadcasts the packet $b_B = d_{AC} \oplus d_{CA}$, where $\oplus$ denotes the bitwise XOR operation. Since the EN A already has d_{AC}, it extracts the required packet d_{CA} through $d_{CA} = b_B \oplus d_{AC}$. Similarly, EN C extracts d_{AC}. The relaying

method shown in Fig. 5.1(b) requires only 3 time slots to transmit the packets d_{AC} and d_{CA}, which means that the bidirectional throughput is "doubled" with respect to the conventional relaying.

5.2.2 Amplify and Forward

In AF relay schemes, the RN is going to amplify the signals from the ENs without decoding, and then forwards it to the destinations [99]. The noisy form of the signal from the ENs is amplified by the relay usually under certain constraints (e.g., power constraint). The resulting signal is transmitted to the destination. The hardware complexity of AF is lower than DF since the decoding function is excluded in AF.

The bidirectional AF relay scheme has been introduced and analyzed in [100] and is different from the usual network coding, since it utilizes the inherent packet combining provided by the multiple access channel. This technique is illustrated in Fig. 5.1(c). Let x_{AC} and x_{CA} be the baseband representations of the packets d_{AC} and d_{CA}, respectively. If in the first slot both ENs A and C are transmitting over the multiple access channel, then RN B receives the noisy version of $y_B = x_{AC} + x_{CA} + z_B$. If RN B amplifies y_B and broadcasts the amplified βy_B, then EN A receives a noisy signal from which it can subtract x_{AC} and attempt to decode x_{CA} (similarly for C). In the absence of noise, A decodes $x_{CA}(d_{CA})$ and C decodes $x_{AC}(d_{AC})$ after only 2 slots, thus doubling the throughput compared to the scheme in Fig. 5.1 (a). However, in the bidirectional AF scheme, the relay node amplifies the noise as well. In the low SNR region, this produces excessive packet errors and thus the obtainable throughput gain

of bidirectional AF diminishes.

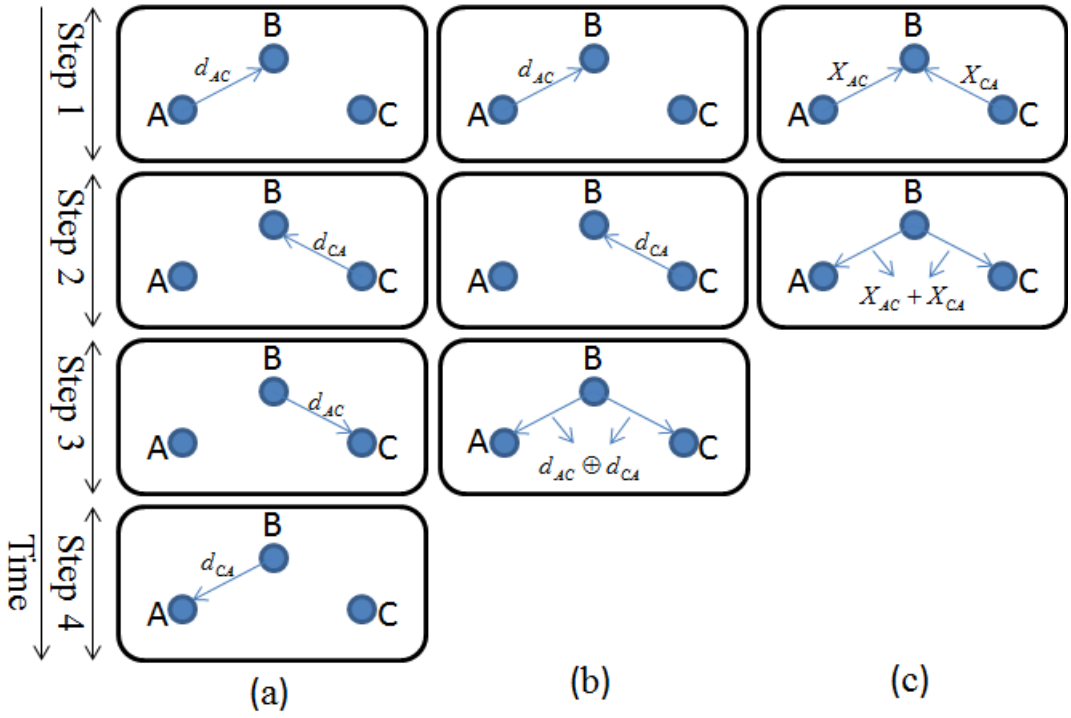

Figure 5.1: Different relay communication methods.

5.2.3 Denoise and Forward

In DNF relay, the RN B does not decode the packets sent by ENs A and C in Step 1. Nevertheless, it can make an estimate $x_B = \hat{d}_{x_{AC}+x_{CA}}$ of $x_{AC}+x_{CA}$ via a decision process that aims to minimize the impact of noise. Hence, the signal x_B now carries the information about the set of codeword pairs $\{(x_{AC}, x_{CA})\}$ which are considered by the RN B as likely to have been sent in Step 1. In general, this set could consist of several codeword pairs; thus RN B has an ambiguity about

what information has been sent. Since $A(C)$ knows $x_{AC}(x_{CA})$, after receiving x_B, it will extract exactly one codeword as a likely one to have been sent by EN $C(A)$ in Step 1.

To avoid confusion, such a decision process is referred to as denoising, instead of decoding. Fig. 5.1(c) can also be used to illustrate the timing for the bidirectional DNF. In absence of channel errors, bidirectional DNF and bidirectional AF perform identically. However, there is a fundamental difference between them in presence of errors: DNF does not amplify the noise, as it broadcasts its estimate $\hat{d}_{x_{AC}+x_{CA}}$ to A and C. Such an operation makes bidirectional DNF superior to the other two bidirectional strategies in terms of achievable throughput. If BPSK modulation is applied, then RN B will receive either $-2, 0$ or

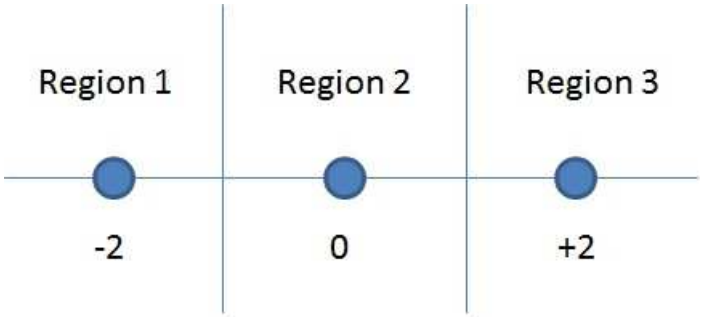

Figure 5.2: DNF bit mapping.

$+2$ for each symbol as depicted in Fig. 5.2. These three possible symbols are mapped to a binary message, indicating either an "equal status" (-2 and $+2$) or an "unequal status" (0). This compression ensures that a combined packet only needs the same amount of bits as a regular packet. At the same time the mapping removes any noise added during transmission, although decoding is not performed. Note that the addition of signals in the air combined with the map-

ping from $-2, 0$ and $+2$ to a binary message is effectively an XOR operation. Equal symbols map to one value and unequal symbols map to another. The final denoised packet is referred to as an analog network coded (ANC) packet. This packet is broadcasted to ENs A and C, which can now reconstruct what was intended for them by performing an XOR operation on the received packet and the packet they transmitted themselves. [95, 100–102]

DNF relay is a way to combine the advantages of the AF and the DF relay schemes. The operation is simple since decoding is not required and the noise is removed. Moreover this scheme inherits the advantage of ANC - the decreased number of necessary transmissions; hence the throughput is increased. The drawback is that it also inherits the disadvantage of ANC - timing synchronization among all the nodes is required. Another drawback is that DNF depends on *a priori* information, which means an end node must be able to save the transmitted packet in order to extract the desired information from the packet broadcasted by the relay node.

The key difference between DNF and other relaying schemes is its special signal processing process at the RN. In DF and AF, the RN either makes very strict bit-level hard decision or simply amplifies the received signals. In the DNF relay scheme, RN denoises the input signals to output signals by using a specially designed multiple-to-one mapping. In this mapping, even if noise causes signal distortion and makes one input similar to another, multiple-to-one mapping can be designed to assign the same output to all these possible inputs, i.e., the distorted input can still yield the same output, thus removing the effect of noise. DNF can be viewed as an alternative to analog AF and digital DF relaying. It retains the advantages of both schemes but overcomes

their disadvantages.

5.3 IR-UWB Relay Assisted Communication Systems

According to the FCC rule, UWB should operate at a transmit power of at most -41.3dBm/MHz to avoid interfering with existing narrow-band communication systems. Due to this limitation, UWB systems face major design challenges in achieving wide coverage while assuring an adequate system performance. Therefore, efficient ways to enhance the system performance are desirable. A possible effective solution is relay-assisted UWB communications. Cooperation via relay represents a new communication paradigm which involves both transmission and distributed processing to increase the capacity and diversity gain in wireless networks [103–107], and to extend the network coverage.

Relay technique as a viable solution for coverage extension has been introduced for UWB networks in [83,109–111] with one-way relay protocols. However, one-way relay extends the coverage of UWB systems at the expense of spectral efficiency loss.

In [114], a PNC aided bi-directional relay scheme, focusing on the detector design, was proposed for TR UWB networks utilizing only one single relay. However, coherent detection based PNC schemes that are used for the narrowband systems [96, 115, 116] may not be appropriate for the low complexity UWB networks, since coherent UWB detection requires complicated channel estimation and stringent signal synchronization.

In order to extend the network coverage, relay techniques with one relay topology were introduced for UWB networks [83, 85, 109, 111] as promising can-

didates for range extension.

IR-UWB communications may be classified into two categories: coherent signaling and non-coherent signaling. Normally, the receiver for coherent signaling requires accurate CSI which is difficult to obtain for highly frequency selective UWB channels. Non-coherent signaling, on the other hand, is much simpler in its receiver structure by avoiding explicit channel estimation. Moreover, digital implementation of UWB receivers requires ultra high analog-to-digital (AD) sampling.

Some novel non-coherent two-way relay schemes have been proposed for UWB networks recently [117, 118]. A cooperative two-way relay scheme is proposed for transmitted reference pulse cluster (TRPC) UWB system [117], which exploits TDMA in the MA phase and the network coded broadcasting (NCBC) in the BC phase. Although TDMA ensures that the data waveforms are orthogonal in the time domain and therefore gets rid of the multiuser interference in the MA phase, the spectral efficiency is lowered. On the other hand, a two-way relay scheme for code multiplexed TR (CMTR) UWB system with PNC, wherein a simple heuristic UWB-PNC detector is developed, but the detector exhibits a relatively high error-floor is proposed in [118]. To our knowledge, there is nearly no existing work on the PNC aided non-coherent two-way relay UWB networks.

5.3.1 Differential Detectors

The transmitted signal in IR-UWB systems can be represented as

$$g(t) = \sum_{k=0}^{N_f-1} a_k w(t - kT_f - c_k T_c)\,, \tag{5.1}$$

where N_f denotes the number of pulses (frames) per symbol, each with duration of T_f, resulting in the symbol time $T_s = N_f T_f$, $a_k \in \{1, -1\}$ is the DS code, $w(t)$ represents the unit-energy transmitted pulse waveform with duration T_p, and c_k is the TH value in the range $0 < c_k < N_h - 1$, where N_h is the total number of the hops which should satisfy $N_h T_c \leq T_f$.

The discrete time impulse response of the UWB channel can be written as $h(t) = \sum_{l=0}^{L-1} \alpha_l \delta(t - \tau_l)$, where α_l is the multipath gain coefficient associated with the l-th path and τ_l is the arrival time of the l-th path. In this case, the received signal is given by

$$r(t) = \sqrt{\varepsilon} \sum_{n=0}^{+\infty} \sum_{l=0}^{L-1} \alpha_l \tilde{s}(n) g(t - nT_s - \tau_l) + \vartheta(t), \tag{5.2}$$

where ε is the transmitted energy per pulse, $\tilde{s}(n) := s(n)\tilde{s}(n-1)$ is the differentially encoded transmitted symbol, and $\vartheta(t)$ is AWGN with variance of σ_ϑ^2.

In the reminder of this thesis, we consider the differential encoding (DE) scheme at the RN and ENs. DE demodulation does not require CSI and nor complicated coherent modulation at the relay. However, there is a performance degradation compared to coherent modulation. A ML differential demodulation technique for UWB communication systems is developed in [112], which is used in our proposed relay schemes. The basic idea of the aforementioned ML

technique is summarized as follows:

i) Forming the received signal $r(t)$ over M symbol periods:

$$r_m(t)=r(t+mT_s), \quad t\in[0,T_s], \;\; m\in[0,M-1]. \tag{5.3}$$

In this case, $r_m(t)$ can be rewritten as

$$r_m(t)=\tilde{s}(m-1)g_{_R}(t-T_s-\tau_0)+\tilde{s}(m)g_{_R}(t-\tau_0)+\vartheta_m(t), \tag{5.4}$$

where $g_{_R}(t)=\sum_{l=0}^{L-1}\alpha_l g(t-\tau_{l,0})$ in which $\tau_{l,0}=\tau_l-\tau_0$.

ii) Correlating corresponding adjacent "dirty" segments $r_m(t)$

$$x(m)=\int_0^{T_s} r_m(t)r_{m-1}(t)dt. \tag{5.5}$$

From (5.3) and (5.4), $x(m)$ is determined as

$$x(m)=\tilde{s}\,(m-1)\,\tilde{s}(m-2)\varepsilon_1+\tilde{s}(m)\tilde{s}(m-1)\varepsilon_2+\xi_m, \tag{5.6}$$

where $\varepsilon_1=\varepsilon\int_{T_s-\tau_0}^{T_s} g_{_R}^2(t)dt$ and $\varepsilon_2=\varepsilon\int_0^{T_s-\tau_0} g_{_R}^2\,(t)\,dt$ are the captured energies of the received waveforms in the period of $[T_s\text{–}\tau_0\;T_s]$ and $[0\;T_s\text{–}\tau_0]$, respectively. ξ_m is the bandpass filtered AWGN [112] with variance $\sigma_\xi=\varepsilon N_0+\frac{{N_0}^2}{4}BT_s$, where B is the bandwidth.

The average power delay profile (APDP) $P_h(t)$ can be approximated as $P_h(t)\approx E\left\{g_{_R}^2(t)\right\}$ [113]. In this case, the average energy of the CIR in a generic time window $\mathcal{W}=[a\;b]$ is obtained as $E\left\{\int_{\mathcal{W}} g_{_R}^2(t)dt\right\}$. By modeling

the APDP as $P_h(t) = \frac{\varepsilon_h}{\tau_{rms}} e^{\frac{-t}{\tau_{rms}}}$ and normalizing the total CIR energy, i.e., $\varepsilon_h = 1$, we can estimate the average captured received energy $E\{\varepsilon_1\}$ and $E\{\varepsilon_2\}$ as

$$\begin{aligned} E\{\varepsilon_1\} &= E\left\{\varepsilon \int_{T_s-\tau_0}^{T_s} g_R^2(t)dt\right\} \approx \varepsilon \int_{T_s-\tau_0}^{T_s} P_h(t)\, dt = \varepsilon\left(e^{-\frac{T_s-\tau_0}{\tau_{rms}}}\right), \\ E\{\varepsilon_2\} &= E\left\{\varepsilon \int_{0}^{T_s-\tau_0} g_R^2(t)dt\right\} \approx \varepsilon \int_{0}^{T_s-\tau_0} P_h(t)\, dt = \varepsilon\left(1 - e^{-\frac{T_s-\tau_0}{\tau_{rms}}}\right). \end{aligned} \tag{5.7}$$

After differential encoding, (5.6) can be rewritten as

$$x(m) = s(m-1)\varepsilon_1 + s(m)\varepsilon_2 + \xi_m. \tag{5.8}$$

iii) Demodulating $s(m)$ and $s(m-1)$ in (5.8).

This part will be explained in more detail in the next section.

5.4 Asynchronous Differential Bidirectional Decode Forward Relay System

Let us consider an ADBDF UWB relay network consisting of two ENs A and C and one RN, B. Namely, two ENs A and C exchange the sequences of information symbols via RN B. The received signals at relay B from two ENs A and C are depicted in Fig. 5.3. Since there is no synchronization between the relay and two ENs, the received signals at the relay have unknown delays τ_{0A} and τ_{0C}. Once the relay receives the signals from the ENs, it applies the differential detection (decoding) technique explained in Sec. 5.3.1 to decode the transmitted sequences. Next, we propose and develop the optimal maximum

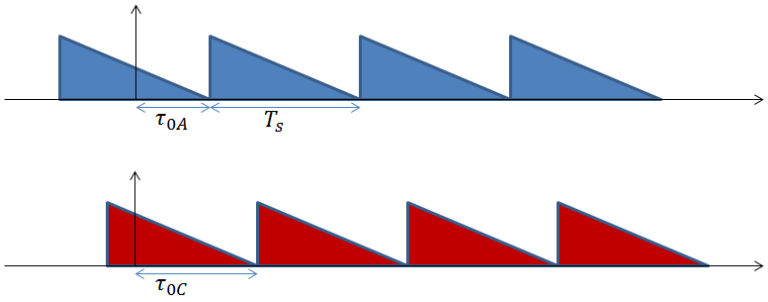

Figure 5.3: Received signals at the relay in ADBDF relay algorithm from two ENs A and C.

likelihood sequence detection (MLSD) and sub-optimal non-coherent demodulation techniques for sequence detection.

5.4.1 Maximum Likelihood Sequence Detection for the Proposed ADBDF Relay Algorithm

Here we investigate MLSD via the Viterbi algorithm to decode/detect the received sequence at the relay for the proposed ADBDF relay scheme. The MLSD technique finds the sequence through the trellis diagram that looks most like the received output sequence. Let us assume that node A transmits data to relay B. The received signal after applying asynchronous differential modulation technique is

$$x_{A}(m) = s_A(m-1)\varepsilon_{1A} + s_A(m)\varepsilon_{2A} + \xi_m. \tag{5.9}$$

The diagram when node A transmits data to the relay B is depicted in Fig 5.4. Each branch in the trellis diagram is labeled with the channel symbol and the corresponding input, i.e., output value/input bit. Also, an error event in the

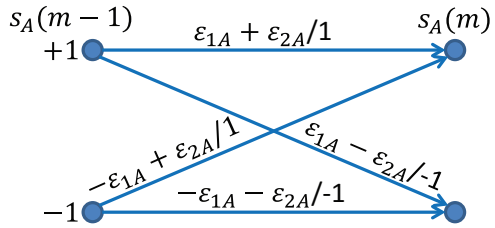

Figure 5.4: Illustration of trellis events diagram for the proposed ADBDF relay algorithm, branch labels =: Output Value/Input Bit.

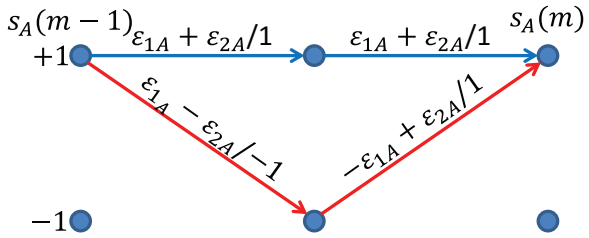

Figure 5.5: Illustration of a trellis error event diagram for the proposed ADBDF relay algorithm.

proposed ADBDF relay algorithm is depicted in Fig. 5.5. The performance of the MLSD via Viterbi is determined by its minimum distance d_{min}, which is defined as the distance between two closest trellis sequences. The corresponding d_{min} for the proposed ADBDF relay scheme is

$$d_{min} = 2\sqrt{\varepsilon_{1A}^2 + \varepsilon_{2A}^2}. \tag{5.10}$$

The nearest neighbor union bound (NNUB)[1] is developed in this chapter to find a bound for the probability of error for the proposed schemes. In this case, the NNUB becomes an approximation of, and not necessarily an upper bound on, the probability of erroneously detecting the sequence transmitted from the relay

[1]NNUB was studied extensively in [113].

B. For the proposed method, the NNUB of $p_A(e)$ is given as

$$\bar{p}_A(e) \leq \bar{N}_e Q\left(\frac{d_{min}}{2\sigma_\xi}\right) = \bar{N}_e Q\left(\frac{\sqrt{\varepsilon_{1A}^2 + \varepsilon_{2A}^2}}{\sigma_\xi}\right), \tag{5.11}$$

where $\bar{N}_e = \sum_i N_i p_i$, N_i is the number of i-th smallest distance occurrences $d(i)$, for all sequences diverging at the same point as $d_{min} = d_{min}(0) < d_{min}(1) < \cdots < d_{min}(i)$ and $p(i)$ is the corresponding probability of occurrences. Therefore, (5.11) can be rewritten as

$$p(\tau_{0A}) < Q\left(\frac{\varepsilon\sqrt{1 - 2e^{\frac{-\tau_{0A}}{\tau_{rms}}} + 2e^{\frac{-2\tau_{0A}}{\tau_{rms}}}}}{\sigma_\xi}\right). \tag{5.12}$$

The average probability of error is obtained as

$$p_A = E\left\{p\left(\tau_{0A}\right)\right\} = \int_0^\infty p_A(\tau_{0A}) f_{T_A}(\tau_{0A})\, d\tau, \tag{5.13}$$

where we assume τ_{0A} has an uniform distribution over $[0\ T_s]$, i.e., $f_{T_A}(\tau_{0A}) = \frac{1}{T_s}$.

Finally, the probability of denoising erroneously the received packet at the relay is

$$p_{p_A} = 1 - (1 - p_A)^N, \tag{5.14}$$

where N is the number of bits in the transmitted packet.

5.4.2 Low-Complexity Conditional ML Differential Detection Scheme for the Proposed ADBDF Relay Algorithm

Under some conditions, a low-complexity algorithm can be employed to demodulate (decode) $s_A(m)$ in (5.9). When $\varepsilon_{1A} \gg \varepsilon_{2A}$, a simple sign-detector demodulation scheme can be applied to demodulate $s_A(m)$ from $x_A(m+1)$. In this case, the probability of detecting $s(m)$ erroneously is

$$p_A(\tau_{0A}) = \frac{1}{4}\left(p\left(x_A(m+1)<0\Big|_{s_A(m-1)=1}^{s_A(m)=1}\right)+p\left(x_A(m+1)<0\Big|_{s_A(m-1)=-1}^{s_A(m)=1}\right)\right.$$
$$\left.+\ p\left(x_A(m+1)>0\Big|_{s_A(m-1)=1}^{s_A(m)=-1}\right)+p\left(x_A(m+1)>0\Big|_{s_A(m-1)=-1}^{s_A(m)=-1}\right)\right), \tag{5.15}$$

where

$$
\begin{aligned}
p\left(x_{_A}(m+1)<0\Big|_{s_A(m-1)=1}^{s_A(m)=1}\right) &= p\left(\varepsilon_{1A}+\varepsilon_{2A}+\xi_{m+1}<0\right) \\
&= Q\left(\frac{\varepsilon}{\sigma_\xi}\right), \\
p\left(x_{_A}(m+1)<0\Big|_{s_A(m-1)=-1}^{s_A(m)=1}\right) &= p\left(\varepsilon_{1A}-\varepsilon_{2A}+\xi_{m+1}<0\right) \\
&= Q\left(\frac{\varepsilon\left(1-2e^{\frac{-\tau_{0A}}{\tau_{rms}}}\right)}{\sigma_\xi}\right), \\
p\left(x_{_A}(m+1)>0\Big|_{s_A(m-1)=1}^{s_A(m)=-1}\right) &= p\left(-\varepsilon_{1A}+\varepsilon_{2A}+\xi_{m+1}>0\right) \\
&= Q\left(\frac{\varepsilon\left(1-2e^{\frac{-\tau_{0A}}{\tau_{rms}}}\right)}{\sigma_\xi}\right), \\
p\left(x_{_A}(m+1)>0\Big|_{s_A(m-1)=-1}^{s_A(m)=-1}\right) &= p\left(-\varepsilon_{1A}-\varepsilon_{2A}+\xi_{m+1}>0\right) \\
&= Q\left(\frac{\varepsilon}{\sigma_\xi}\right).
\end{aligned}
\tag{5.16}
$$

Hence, $p_A(\tau_{0A})$ is given as

$$
p_A(\tau_{0A}) = \frac{1}{2}Q\left(\frac{\varepsilon\left(1-2e^{\frac{-\tau_{0A}}{\tau_{rms}}}\right)}{\sigma_\xi}\right)+\frac{1}{2}Q\left(\frac{\varepsilon}{\sigma_\xi}\right). \tag{5.17}
$$

In Appendix A, $E\left[p\left(\tau_{0A}\right)\right]$ is derived as

$$E\left[p(\tau_{0A})\right] = \frac{1}{4} - \sqrt{\frac{2}{\pi}}\frac{\tau_{rms}}{2T_s}\sum_{n=0}^{\infty}\sum_{m=0}^{\infty}\binom{2n+1}{m}\left(\frac{\varepsilon}{\sigma_\xi}\right)^{2n+1}\frac{(-2)^{n-m}\,\alpha^m\beta^{2n+1-m}}{n!\,(2n+1)\,(2n+1-m)} \times\left(e^{\frac{-T_s(2n+1-m)}{\tau_{rms}}}-1\right)+\frac{1}{2}Q\left(\frac{\varepsilon}{\sigma_\xi}\right). \tag{5.18}$$

Finally, the packet error rate (PER) at the relay can be calculated from (5.14).

5.4.3 Parameter Estimation

Since there is no channel estimation at the relay, the received energies at the relay, ε_{1A} and ε_{2A}, are unknown, and an estimation algorithm should be applied to estimate them. A simple technique is to send a training sequence such that at the relay we have

$$\begin{aligned} x_1(m) &= \varepsilon_{1A}+\varepsilon_{2A}+\xi_{1m}, \\ x_2(m) &= \varepsilon_{1A}-\varepsilon_{2A}+\xi_{2m}. \end{aligned} \tag{5.19}$$

In this case, the estimates of ε_{1A} and ε_{2A} can be derived as $\hat{\varepsilon}_{1A} = \varepsilon\left(1-e^{\frac{-\tau_{0A}}{\tau_{rms}}}\right)$ and $\hat{\varepsilon}_{2A} = \varepsilon\left(e^{\frac{-\tau_{0A}}{\tau_{rms}}}\right)$, respectively. We propose another algorithm to estimate ε_{1A} and ε_{2A}, which is based on the statistical information of the received signal. The second and fourth moments of the noise-free received signal from EN A can

be given as

$$\begin{aligned} E\{x_A^2(m)\} &= \varepsilon_{1A}^2 + \varepsilon_{2A}^2, \\ E\{x_A^4(m)\} &= \varepsilon_{1A}^4 + \binom{4}{2}\varepsilon_{1A}^2\varepsilon_{2A}^2 + \varepsilon_{2A}^4. \end{aligned} \tag{5.20}$$

However, the aforementioned technique leads to two symmetric solution sets, i.e., $(\varepsilon_{1A}, \varepsilon_{2A}) = (\gamma, \omega)$ or $(\varepsilon_{1A}, \varepsilon_{2A}) = (\omega, \gamma)$, where only one of them is correct. In order to determine the correct solution set, we propose a new technique that compares the following metrics (cost functions)

$$\begin{aligned} C_{k_1} &= \sum_{m=0}^{k-1} |x_A(m) - s_A(m-1)\gamma - s_A(m)\omega|^2, \\ C_{k_2} &= \sum_{m=0}^{k-1} |x_A(m) - s_A(m-1)\omega - s_A(m)\gamma|^2, \end{aligned} \tag{5.21}$$

where k is the length of the sequence for the cost function input. The metric with the minimum value is chosen as a metric that has the correct solution set for ε_{1A} and ε_{2A}. In our algorithm even though the two ENs are not synchronized with the RN, in the initializing step, in order to estimate $(\hat{\varepsilon}_{1A}, \hat{\varepsilon}_{2A})$, $(\hat{\varepsilon}_{1C}, \hat{\varepsilon}_{2C})$, the RN receives packets from each EN in a timely manner. Once these parameters are estimated, the two ENs can transmit their data simultaneously in the next step. From the estimated parameters, a coarse timing acquisition algorithm based on the statistical properties of the UWB channel is obtained.

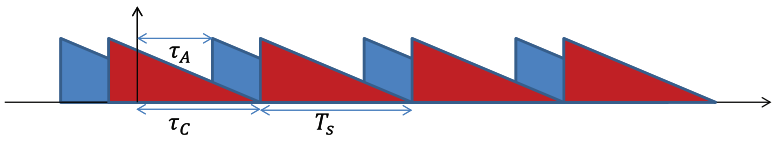

Figure 5.6: Received signal at the relay in asynchronous DNF relay algorithm.

5.5 Asynchronous Differential Bidirectional Denoise and Forward Relay System

In the proposed ADBDNF relay scheme the ENs transmit their data simultaneously to the RN. However, the RN does not decode the received data individually. The whole procedure of the DNF relay algorithm can be summarized in two steps. In the first step, the ENs A and C send X_{AC} and X_{CA} packets to the RN B simultaneously and in the next step, the RN estimates $\hat{d}_{X_{AC}+X_{CA}}$. The received signal from two ENs A and C at the relay B is depicted in Fig. 5.6. The received signal at the relay in the DNF relay method is

$$\begin{aligned} r_m(t) = {} & \tilde{s}_A(m-1)g_{R_A}(t-T_s-\tau_{0A}) + \tilde{s}_A(m)g_{R_A}(t-\tau_{0A}) \\ & + \tilde{s}_C(m-1)g_{R_C}(t-T_s-\tau_{0C}) + \tilde{s}_C(m)g_{R_C}(t-\tau_{0C}) \\ & + \vartheta_m(t). \end{aligned} \tag{5.22}$$

The correlation of the segmented signal is calculated in (5.5). Without loss of generality, we assume $\tau_{0A} < \tau_{0C}$; similar equations can be derived when $\tau_{0A} > \tau_{0C}$. By defining $\varepsilon_{1A} = \int_{T_s-\tau_{0A}}^{T_s} g_{R_A}^2(t)\,dt$ and $\varepsilon_{2A} = \int_0^{T_s-\tau_{0A}} g_{R_A}^2(t)\,dt$ and

similar equations for ε_{1C} and ε_{2C}, we have

$$\begin{aligned} x(m) = {} & s_A(m-1)\varepsilon_{1A}+s_A(m)\varepsilon_{2A}+s_C(m)\varepsilon_{1C}+s_C(m-1)\varepsilon_{2C} \\ & + \left(\tilde{s}_A(m-1)\tilde{s}_C(m-2) + \tilde{s}_A(m-2)\tilde{s}_C(m-1)\right)\varepsilon_{1_{AC}} \\ & + \left(\tilde{s}_A(m)\tilde{s}_C(m-2)+\tilde{s}_A(m-1)\tilde{s}_C(m-1)\right)\varepsilon_{2_{AC}} \\ & + \left(\tilde{s}_A(m)\tilde{s}_C(m-1) + \tilde{s}_A(m-1)\tilde{s}_C(m)\right)\varepsilon_{3_{AC}} \\ & + \xi_m, \end{aligned} \tag{5.23}$$

where $\varepsilon_{1_{AC}}$, $\varepsilon_{2_{AC}}$, and $\varepsilon_{3_{AC}}$ are interfered-received-pulses cross correlation (IRP-CC) and can be calculated as

$$\begin{aligned} \varepsilon_{1_{AC}} &= \int_0^{\tau_{0A}} g_{R_A}(t+T_s-\tau_{0A})g_{R_C}(t+T_s-\tau_{0C})\,dt, \\ \varepsilon_{2_{AC}} &= \int_{\tau_{0A}}^{\tau_{0C}} g_{R_A}(t-\tau_{0A})g_{R_C}(t+T_s-\tau_{0C})\,dt, \\ \varepsilon_{3_{AC}} &= \int_{\tau_{0C}}^{T_s} g_{R_A}(t-\tau_{0A})g_{R_C}(t-\tau_{0C})\,dt. \end{aligned} \tag{5.24}$$

The expected value of $\varepsilon_{1_{AC}}$ is derived as

$$E\left\{\varepsilon_{1_{AC}}\right\} = E\left\{\int_0^{\tau_{0A}} g_{R_A}(t+T_s-\tau_{0A})g_{R_C}(t+T_s-\tau_{0C})dt\right\}. \tag{5.25}$$

Since $E\left\{g_{R_A}(t+T_s-\tau_{0A})\right\} = E\left\{g_{R_C}(t+T_s-\tau_{0C})\right\} = 0$ and the received signal from the ENs A and C are independent (or at least uncorrelated), it follows $E\{\varepsilon_{1_{AC}}\} = 0$. Similarly, we have $E\left\{\varepsilon_{2_{AC}}\right\} = E\left\{\varepsilon_{3_{AC}}\right\} = 0$. The variance of IRP-CC is derived in [113] as

$$var\left\{\int_{\mathcal{A}} g_{R_A}(t)g_{R_C}(t+\tau)dt\right\} = \int_{-\infty}^{\infty}\phi^2(t)dt\int_{\mathcal{A}} P_h^{(A)}(t)P_h^{(C)}(t+\tau)dt, \tag{5.26}$$

where $\phi(\tau) = \int_{-\infty}^{\infty} w_{_T}(t) w_{_T}(t+\tau)\, dt$. By normalizing $\phi(\tau)$, i.e., $\phi(0) = 1$, we have

$$\begin{aligned}
var\{\varepsilon_{1_{AC}}\} &= \frac{1}{2} c_1 \frac{\varepsilon^2}{\tau_{rms}} e^{-\left(\frac{\tau_{0A}-\tau_{0C}}{\tau_{rms}}\right)} \left(e^{\frac{-2(T_s-\tau_{0A})}{\tau_{rms}}} - e^{\frac{-2T_s}{\tau_{rms}}} \right), \\
var\{\varepsilon_{2_{AC}}\} &= \frac{1}{2} c_1 \frac{\varepsilon^2}{\tau_{rms}} e^{-\left(\frac{T_s+\tau_{0A}-\tau_{0C}}{\tau_{rms}}\right)} \left(1 - e^{\frac{-2(\tau_{0C}-\tau_{0A})}{\tau_{rms}}} \right), \\
var\{\varepsilon_{3_{AC}}\} &= \frac{1}{2} c_1 \frac{\varepsilon^2}{\tau_{rms}} e^{-\left(\frac{\tau_{0A}-\tau_{0C}}{\tau_{rms}}\right)} \left(e^{\frac{-2(\tau_{0C}-\tau_{0A})}{\tau_{rms}}} - e^{\frac{-2(T_s-\tau_{0A})}{\tau_{rms}}} \right),
\end{aligned} \tag{5.27}$$

where $c_1 \approx 0.0153\tau_{rms}$. We can also show that $var\{\tilde{s}_A(m-1)\tilde{s}_C(m-2) + \tilde{s}_A(m-2)\tilde{s}_C(m-1)\} = var\{\tilde{s}_A(m)\tilde{s}_C(m-2) + \tilde{s}_A(m-1)\tilde{s}_C(m-1)\} = var\{\tilde{s}_A(m)\tilde{s}_C(m-1) + \tilde{s}_A(m-1)\tilde{s}_C(m)\} = 2$ and

$$\begin{aligned}
\xi_m = \int_0^{T_s} \vartheta_{m-1}(t) \Big(& \tilde{s}_A(m-1) g_{_{R_A}}(t - T_s - \tau_{0A}) + \tilde{s}_A(m) g_{_{R_A}}(t - \tau_{0A}) \\
& + \tilde{s}_C(m-1) g_{_{R_C}}(t - T_s - \tau_{0C}) + \tilde{s}_C(m) g_{_{R_C}}(t - \tau_{0C}) + \vartheta_m(t) \Big) dt.
\end{aligned} \tag{5.28}$$

In this case, $var\,\{\xi_m\}$ can be given as

$$var\,\{\xi_m\} = \varepsilon N_0 + \frac{{N_0}^2}{4} B T_s. \tag{5.29}$$

Hence, the total variance of the IRP-CC is

$$\begin{aligned}
\sigma_T^2(\tau_{0C}, \tau_{0A}) &= 2\Big(var\{\varepsilon_{1_{AC}}\} + var\{\varepsilon_{2_{AC}}\} + var\{\varepsilon_{3_{AC}}\} \Big) + var\,\{\xi_m\} \\
&\approx c_1 \frac{\varepsilon^2}{\tau_{rms}} \left(e^{\frac{-(T_s+\tau_{0A}-\tau_{0C})}{\tau_{rms}}} - e^{\frac{-(\tau_{0C}-\tau_{0A})}{\tau_{rms}}} \right) + \varepsilon N_0 + \frac{{N_0}^2}{4} B T_s.
\end{aligned} \tag{5.30}$$

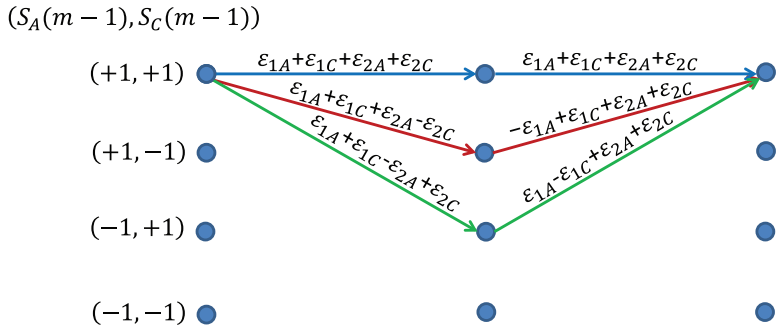

Figure 5.7: Illustration of trellis error events diagram for the proposed ADBDNF relay algorithm, branch labels =: Output Value.

5.5.1 Maximum Likelihood Sequence Detection Scheme for the Proposed ADBDNF Relay Algorithm

In this section the Viterbi algorithm applied in the proposed ADBDNF relay method to decode the transmitted sequences is explained. An error event for the proposed ADBDNF relay scheme is depicted in Fig. 5.7. In this case, d_{min} can be calculated as

$$d_{min} = \begin{cases} 2\sqrt{\varepsilon_{1A}^2 + \varepsilon_{2A}^2} & \tau_{0A} < \tau_{0C} \\ 2\sqrt{\varepsilon_{1C}^2 + \varepsilon_{2C}^2} & \tau_{0A} > \tau_{0C} \end{cases}. \tag{5.31}$$

Therefore, from (5.11), (5.30), and (5.31) an approximation of the the MLSD error probability is bounded as

$$p(e|\tau_{0A} < \tau_{0C}) < Q\left(\sqrt{\frac{\varepsilon_{1A}^2 + \varepsilon_{2A}^2}{\sigma_T^2(\tau_{0C}, \tau_{0A})}}\right). \tag{5.32}$$

A simplified approximation can be derived by assuming that the total captured energy from the two ENs are fixed and equal, i.e., $\varepsilon_{1A}+\varepsilon_{2A}=\varepsilon_{1C}+\varepsilon_{2C}=\varepsilon$. In this case, we have $\frac{\varepsilon^2}{2}<\varepsilon_{1A}^2+\varepsilon_{2A}^2<\varepsilon^2$. Also, by the fact that when $\tau_{0A}<\tau_{0C}$, $\sigma_T^2\left(\tau_{0C},\tau_{0A}\right)\leq c_1\frac{\varepsilon^2}{\tau_{rms}}\left(1-e^{-\frac{T_s}{\tau_{rms}}}\right)+var\left\{\xi_m\right\}$, a bound for (5.32) can be given as a simplified approximation can be derived by assuming that the total captured energy from the two ENs are fixed and equal, i.e., $\varepsilon_{1A}+\varepsilon_{2A}=\varepsilon_{1C}+\varepsilon_{2C}=\varepsilon$. Therefore, we have $\frac{\varepsilon^2}{2}<\varepsilon_{1A}^2+\varepsilon_{2A}^2<\varepsilon^2$. Also, by the fact that when $\tau_{0A}<\tau_{0C}$, $\sigma_T^2\left(\tau_{0C},\tau_{0A}\right)\leq c_1\frac{\varepsilon^2}{\tau_{rms}}\left(1-e^{-\frac{T_s}{\tau_{rms}}}\right)+var\left\{\xi_m\right\}$, a bound for (5.32) is given as

$$\begin{aligned} p\left(e|\tau_{0A}<\tau_{0C}\right) &< Q\left(\sqrt{\frac{\varepsilon_{1A}^2+\varepsilon_{2A}^2}{\sigma_T^2(\tau_{0C},\tau_{0A})}}\right)<Q\left(\sqrt{\frac{\varepsilon^2/2}{\sigma_T^2\left(\tau_{0C},\tau_{0A}\right)}}\right) \\ &< Q\left(\sqrt{\frac{\varepsilon^2/2}{c_1\frac{\varepsilon^2}{\tau_{rms}}\left(1-e^{-\frac{T_s}{\tau_{rms}}}\right)+var\left\{\xi_m\right\}}}\right). \end{aligned} \tag{5.33}$$

To find $E\left\{p\left(e|\tau_{0A}<\tau_{0C}\right)\right\}$, we define $\varepsilon_{1A}=x$ and $\varepsilon_{2A}=y$. Hence, we have

$$\begin{aligned} E\left\{p(e|\tau_{0A}<\tau_{0C})\right\} &= E\left\{Q\left(\sqrt{\frac{\varepsilon_{1A}^2+\varepsilon_{2A}^2}{\sigma_T^2\left(\tau_{0C},\tau_{0A}\right)}}\right)\right\} \\ &= \int_0^\infty\int_0^\infty Q\left(\sqrt{\frac{x^2+y^2}{\sigma_T^2\left(\tau_{0C},\tau_{0A}\right)}}\right)f_{X,Y}(x,y)\,dx\,dy \\ &< Q\left(\sqrt{\frac{\varepsilon^2/2}{\sigma_T^2\left(\tau_{0C},\tau_{0A}\right)}}\right). \end{aligned} \tag{5.34}$$

Therefore, the average MLSD error probability is

$$p=p(\tau_{0A}<\tau_{0C})E\left\{p(e|\tau_{0A}<\tau_{0C})\right\}+p(\tau_{0C}<\tau_{0A})E\left\{p(e|\tau_{0C}<\tau_{0A})\right\}. \tag{5.35}$$

We suppose the events $(\tau_{0A} < \tau_{0C})$ and $(\tau_{0C} < \tau_{0A})$ are equally probable, i.e., $p(\tau_{0A} < \tau_{0C}) = p(\tau_{0C} < \tau_{0A}) = 0.5$. Hence we have

$$p = \frac{1}{2}\left(E\left\{p\left(e|\tau_{0A} < \tau_{0C}\right)\right\} + E\left\{p\left(e|\tau_{0C} < \tau_{0A}\right)\right\}\right). \tag{5.36}$$

In this case, the average PER at the relay is given by

$$p_r = 1 - (1-p)^N. \tag{5.37}$$

In the DF relay method, since the two ENs do not transmit data simultaneously, the received symbols at relay from the two ENs do not interfere with each other. However, in the DNF relay scheme, two ENs transmit data simultaneously and when timing synchronization between the ENs and the relay (the case that we assume here) is not perfect, the received signals from the two ENs interfere with each other at the relay. A comprehensive statistical analysis of UWB channel correlation is available in [113]. It is shown that the cross correlation function (CCF) of the received pulses can be modeled as an exponential function.

5.5.2 Low-Complexity Conditional ML Differential Detection Relay Scheme for the Proposed DNF Relay Algorithm

Since in the DNF relay technique we are only interested in detecting the sign of the received symbols at the relay, a low-complexity sign-detector can be employed to obtain the sign of $\{s_A(m)s_C(m)\}$. In this case, the probability of

denoising $sign\{s_A(m)s_C(m)\}$ erronously in (5.23) is given by

$$\begin{aligned} p\left(e|\tau_{0A} > \tau_{0C}\right) &= p\left(x\left(m+1\right) < \frac{\varepsilon_{1A}}{2}\Big|_{s_C(m)=1}^{s_A(m)=1}\right), \\ p\left(e|\tau_{0C} > \tau_{0A}\right) &= p\left(x\left(m+1\right) < \frac{\varepsilon_{1C}}{2}\Big|_{s_C(m)=1}^{s_A(m)=1}\right), \end{aligned} \tag{5.38}$$

which can be expanded as

$$\begin{aligned} p\left(x\left(m+1\right) < \frac{\varepsilon_{1A}}{2}\Big|_{s_C(m)=1}^{s_A(m)=1}\right) = \frac{1}{4}\Bigg(Q\left(\varepsilon\frac{\frac{3}{2}+\frac{1}{2}e^{\frac{-\tau_{0A}}{\tau_{rms}}}}{\sigma_T^2\left(\tau_{0C},\tau_{0A}\right)}\right) + Q\left(\varepsilon\frac{\frac{3}{2}+\frac{1}{2}e^{\frac{-\tau_{0A}}{\tau_{rms}}}-2e^{\frac{-\tau_{0C}}{\tau_{rms}}}}{\sigma_T^2\left(\tau_{0C},\tau_{0A}\right)}\right) \\ +Q\left(\varepsilon\frac{\frac{3}{2}-\frac{3}{2}e^{\frac{-\tau_{0A}}{\tau_{rms}}}}{\sigma_T^2\left(\tau_{0C},\tau_{0A}\right)}\right) + Q\left(\varepsilon\frac{\frac{3}{2}-\frac{3}{2}e^{\frac{-\tau_{0A}}{\tau_{rms}}}-2e^{\frac{-\tau_{0C}}{\tau_{rms}}}}{\sigma_T^2\left(\tau_{0C},\tau_{0A}\right)}\right)\Bigg). \end{aligned} \tag{5.39}$$

$$\begin{aligned} p\left(x\left(m+1\right) < \frac{\varepsilon_{1C}}{2}\Big|_{s_C(m)=1}^{s_A(m)=1}\right) = \frac{1}{4}\Bigg(Q\left(\varepsilon\frac{\frac{3}{2}+\frac{1}{2}e^{\frac{-\tau_{0C}}{\tau_{rms}}}}{\sigma_T^2\left(\tau_{0C},\tau_{0A}\right)}\right) + Q\left(\varepsilon\frac{\frac{3}{2}+\frac{1}{2}e^{\frac{-\tau_{0A}}{\tau_{rms}}}-2e^{\frac{-\tau_{0A}}{\tau_{rms}}}}{\sigma_T^2\left(\tau_{0C},\tau_{0A}\right)}\right) \\ +Q\left(\varepsilon\frac{\frac{3}{2}-\frac{3}{2}e^{\frac{-\tau_{0C}}{\tau_{rms}}}}{\sigma_T^2\left(\tau_{0C},\tau_{0A}\right)}\right) + Q\left(\varepsilon\frac{\frac{3}{2}-\frac{3}{2}e^{\frac{-\tau_{0C}}{\tau_{rms}}}-2e^{\frac{-\tau_{0A}}{\tau_{rms}}}}{\sigma_T^2\left(\tau_{0C},\tau_{0A}\right)}\right)\Bigg). \end{aligned} \tag{5.40}$$

In this case, p_r can be calculated by (5.35), (5.36), and (5.37).

5.6 Throughput Analysis

In this section the throughputs of the proposed methods are calculated and compared with the ideal case, i.e., synchronous links between the ENs and the relay exists, and with the conventional relaying scheme. To compare the through-

put of the proposed algorithms, first, the Markov model of each relay scheme is presented and then the throughput of the corresponding scheme is calculated.

5.6.1 Conventional Relay Scheme

The Markov chain model of the conventional method is depicted in Fig. 5.8(a), with the following states:

S_0: Relay B is empty and node A is going to send its data to the relay;

S_1: Relay B has received data from node A;

S_2: Relay B is empty and node C is going to send its data to the relay;

S_3: Relay B has received the data from node C.

$$\begin{aligned} p(S_0) &= p(S_0)p_{p_A} + p(S_3)(1-p_{p_A}), \\ p(S_1) &= p(S_0)(1-p_{p_A}) + p(S_1)p_{p_C}, \\ p(S_2) &= p(S_1)(1-p_{p_A}) + p(S_2)p_{p_C}, \\ p(S_0) &+ p(S_1) + p(S_2) + p(S_3) = 1, \end{aligned} \tag{5.41}$$

where p_{p_A} and p_{p_C} are the PER for the links $A \to B$ and $C \to B$, respectively, which are given by (5.14). The throughput of the conventional relay scheme is proportional to the non-empty states probabilities, i.e., $p(S_0)$ and $p(S_1)$ and is given as

$$\begin{aligned} R_{Conv}(p_A, p_C) &= R_s \left(p\left(S_1\right)\left(1-p_{p_C}\right) + p\left(S_3\right)\left(1-p_{p_A}\right)\right) \\ &= R_s \frac{\left(1-p_{p_A}\right)\left(1-p_{p_C}\right)}{2-p_A-p_{p_C}}, \end{aligned} \tag{5.42}$$

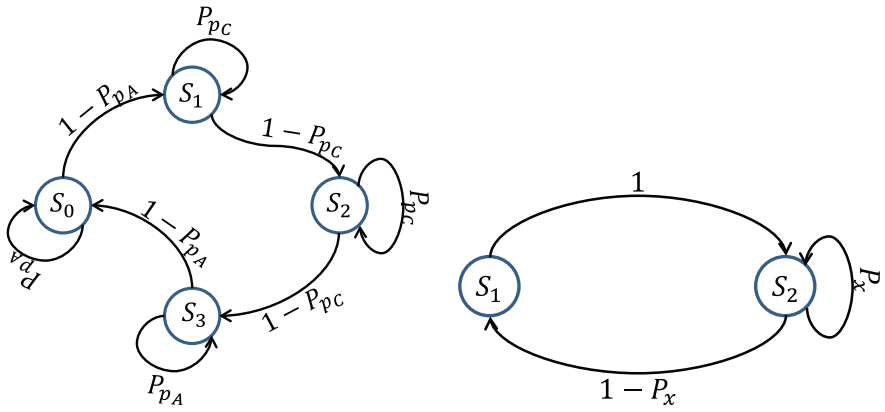

(a) Conventional relay. (b) ADBDNF relay.

Figure 5.8: Markov chain model of the conventional and ADBDNF relay schemes.

where R_s is the data rate, $p(S_0)=\frac{1-p_{p_A}}{2\left(2-p_{p_A}-p_{p_C}\right)}$ and $p(S_1)=\frac{1-p_{p_C}}{2(2-p_{p_A}-p_{p_C})}$.

5.6.2 ADBDF Relay Scheme

The throughput of the DF scheme was studied comprehensively in [95] and is derived as

$$R_{ADBDF}=R_s\frac{(2-p_{p_A}-p_{p_C})(1-p_{p_A})(1-p_{p_C})}{3-3p_{p_A}-3p_{p_C}+p_{p_A}p_{p_C}+p_{p_A}^2+p_{p_C}^2}. \tag{5.43}$$

5.6.3 ADBDNF Relay Scheme

The throughput of the ADBDNF relay method can be analyzed by its Markov chain model illustrated in Fig. 5.8(b). Let $p(S_0)$ be the probability that the relay is empty, $p(S_1)$ the probability that the relay is full, and p_x the probability of denoising erroneously the received packet at the relay. The following

relationships hold

$$\begin{aligned} p(S_0)+p(S_1)p_x &= p(S_1), \\ p(S_0)+p(S_1) &= 1, \end{aligned} \tag{5.44}$$

and

$$p_x = p_r(1-p_{p_A})(1-p_{p_C})+p_{p_A}p_{p_C}p_r+p_{p_A}(1-p_{p_C})(1-p_r)+p_{p_C}(1-p_{p_A})(1-p_r), \tag{5.45}$$

where p_r is given by (5.37). The throughput of the ADBDNF relay method is proportional to $p(S_1)$ and is given by

$$\begin{aligned} R_{ADBDNF} &= R_s p(S_1)(1-p_x) \\ &= 2R_s\left(\frac{1-p_x}{2-p_x}\right). \end{aligned} \tag{5.46}$$

5.7 Numerical Evaluation

In this section, we investigate the throughput performances of the proposed relaying schemes in LOS and NLOS environments. We analyze the throughput performance in two different scenarios. In the first scenario, the Viterbi algorithm is employed to demodulate/detect the received signal at the relay, and in the second scenario, a low-complexity sign-detector is employed at the relay. We also compare the performance of the proposed schemes with that of the synchronous differential demodulation scheme.

As it is clearly seen in Fig. 5.9 and Fig. 5.10, the synchronous differential schemes have the best performance among all schemes. However, when low-

complexity/low-cost systems are desirable, our proposed schemes are the ideal candidates. Synchronous differential demodulation relay schemes have the highest throughput performance compared to other schemes. An abnormal behavior in throughput performance for the proposed ADBDNF is circled in Fig. 5.9. The main reason causing this abnormal behavior is interference at the relay. Since in ADBDNF relay scheme both ENs transmit data simultaneously, interference occurs at the relay. However, as explained in Sec. 5.5, due to the nature of the UWB signals, the interference can be modeled as the cross-correlation between two independent UWB signals whose variances are negligible compared to the signal power.

It is also seen from Fig. 5.9 and Fig. 5.10 that the throughput performance in LOS environment is better than in the NLOS environments, since τ_{rms} in LOS channels is smaller than τ_{rms} in NLOS channels. Our simulation is based on the IEEE 802.15.4a and for LOS channels $\tau_{rms} = 4.11$ ns; for NLOS channels $\tau_{rms} = 16.77$ ns.

Another important parameter that significantly affects the throughput performance is the length of the packets. As depicted in Fig. 5.11 and Fig. 5.12, when the length of the packets is $N = 1000$ the throughput performance is degraded compared with the performance shown in Fig. 5.9 and Fig. 5.10 with a packet length $N = 100$.

5.8 Conclusion

Asynchronous, differential, and bidirectional relay schemes for UWB communication systems in LOS/NLOS environments are proposed in this chapter. The

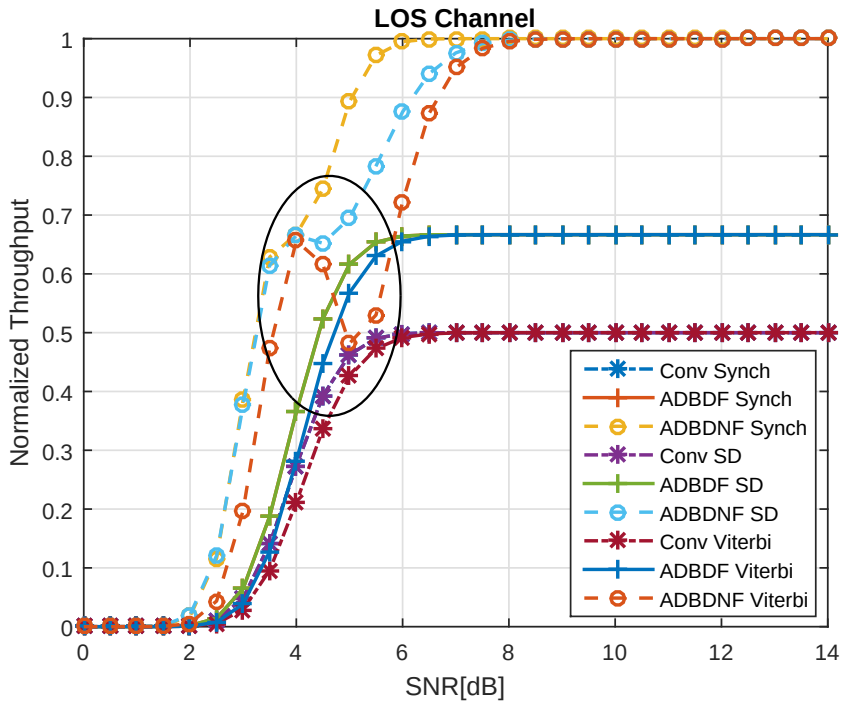

Figure 5.9: Throughput performance of ADBDF, ADBDNF, and conventional relay schemes for $N = 100$ for LOS channels.

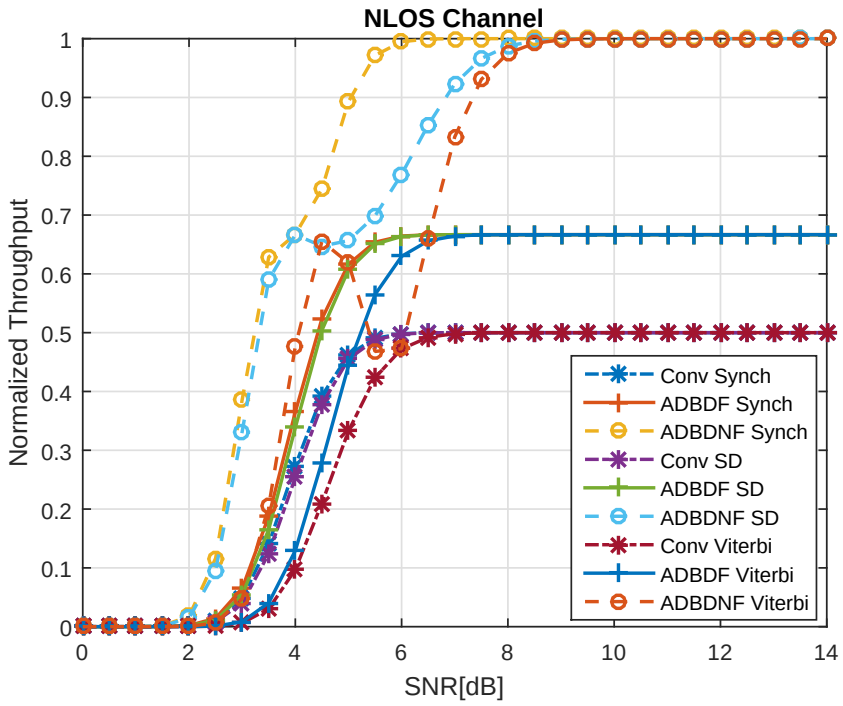

Figure 5.10: Throughput performance of ADBDF, ADBDNF, and conventional relay schemes for $N = 100$ for NLOS channels.

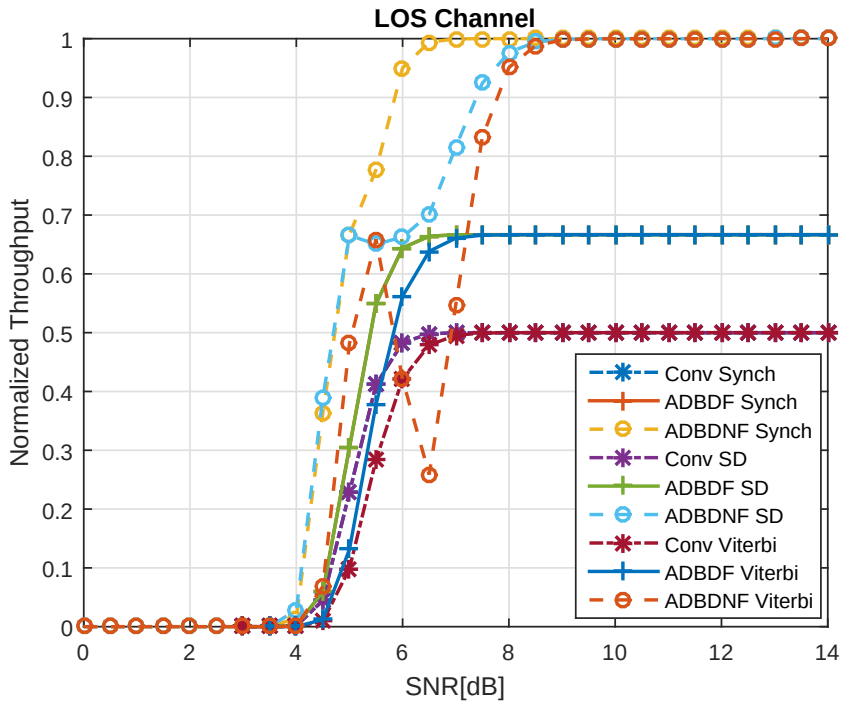

Figure 5.11: Throughput performance of ADBDF, ADBDNF, and conventional relay schemes for $N = 1000$ for LOS channels.

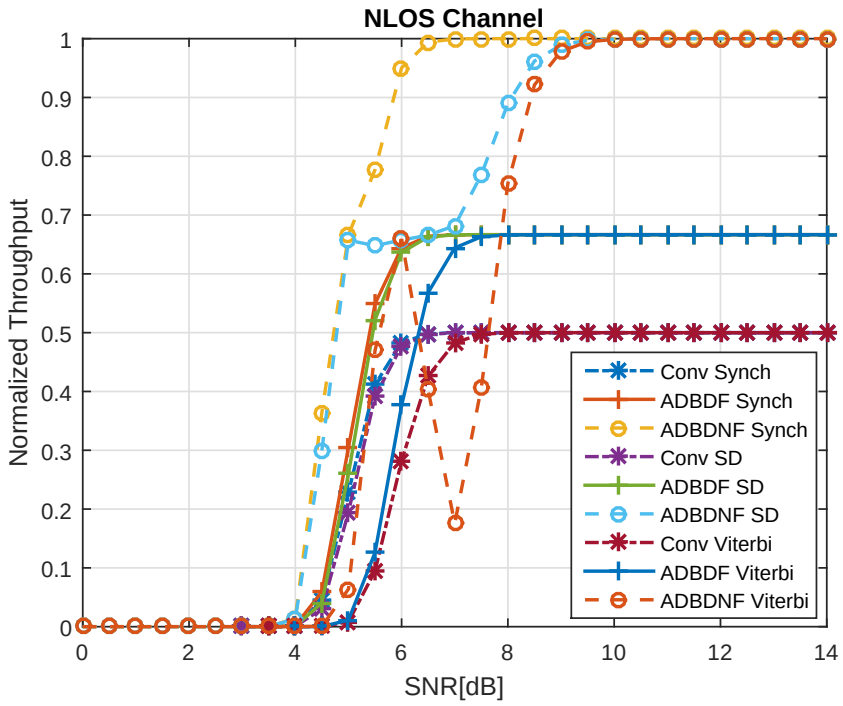

Figure 5.12: Throughput performance of ADBDF, ADBDNF, and conventional relay schemes for $N = 1000$ for NLOS channels.

proposed algorithms can be also employed in synchronous scenarios where optimum performance can be achieved. The proposed schemes do not require timing synchronization and channel estimation, which are complex to maintain or obtain, and are thus appropriate for practical UWB relay networks. By efficiently exploiting the properties of pulsed UWB signals, in the ADBDNF relay scheme, even though the ENs are not time synchronized and the received signals at the relay interfere with each other, the interferences diminish rapidly because their cross-correlation reduces sharply as a function of their time differences. Consequently, the throughput performance is still very good. A new closed-form expression that can be used to solve integrals that involve the Q-function analytically is developed in this chapter. The throughput performances of the proposed schemes are derived by using this new expression. The proposed schemes and the conventional relay scheme are compared under different parameters and also with the case of a synchronous link between the ENs and the relay.

Chapter 6 – Conclusion and Future Work

6.1 Conclusion

This dissertation proposes solutions to address the technical challenges associated with three main areas of UWB communication systems: (1) LOS/NLOS channel classification; and (2) relay-assisted UWB communication systems; and (3) high sampling rate of UWB signals due to their huge bandwidth. We have proposed novel solutions to solve these problems.

First, a novel 2-dimensional UWB channel classification is proposed to identify NLOS channel conditions with a higher accuracy and lower complexity than existing schemes. The proposed scheme employs the skewness as a statistical parameter in channel classification, and is shown to decrease the channel identification ambiguity and improve channel classification probability.

Secondly, we have proposed two novel UWB bi-directional relay-assisted communication systems where the relay employs non-coherent differential demodulation schemes to demodulate the received sequences. It is shown that with the proposed scheme, even though the end nodes and the relay node operate asynchronously, differential demodulation can be employed in the relay while still achieving a good performance.

Thirdly, we have developed a novel compressive sensing based UWB channel estimation algorithm. A coarse graining technique that can be applied in comprehensive sensing theory to reduce the sampling rate while still maintaining a

good performance is proposed.

6.2 Future Work

In the area of relay communications, only one relay is considered in the relay communications cases in this thesis. Extending the proposed schemes to a more general case of UWB communications with multiple relays and with higher-order modulation will be very useful. The proposed LOS/NLOS classification schemes can be applied in cooperative UWB relay communication systems to improve performance. When the link/channel between the EN and the RN If NLOS is identified, the link may be left idle until the link improves to a LOS link. This will improve the network performance drastically.

Chapter 7 – Appendix

Calculating $E\left\{erf\left(\alpha+\beta e^{\frac{-\tau_{0A}}{\tau_{rms}}}\right)\right\}$ over a uniform distribution with $f_{T_A}=\frac{1}{\tau_{0A}}$. By representing Q-function as

$$Q(x)=\frac{1}{2}-\frac{1}{2}erf\left(\frac{x}{\sqrt{2}}\right), \tag{7.1}$$

where

$$erf(x)=\frac{2}{\sqrt{\pi}}\sum_{n=0}^{\infty}\frac{(-1)^n x^{2n+1}}{n!(2n+1)}. \tag{7.2}$$

and after some manipulations, a new closed-form expression to get the average of $Q(\frac{a\tau+\gamma\varepsilon_R}{\sigma_\xi})$ over the uniform distribution $f_{\tau_{0A}}(\tau_{0A})=\frac{1}{T_s}$ can be derived as

$$erf\left(\alpha+\beta e^{x}\right)=\frac{2}{\sqrt{\pi}}\sum_{n=0}^{\infty}\sum_{m=0}^{\infty}\binom{2n+1}{m}\frac{(-1)^n\,\alpha^m\beta^{2n+1-m}}{n!\,(2n+1)}\left(e^{x}\right)^{2n+1-m}. \tag{7.3}$$

$$\int_a^b erf\left(\alpha+\beta e^{x}\right)dx=\frac{2}{\sqrt{\pi}}\sum_{n=0}^{\infty}\sum_{m=0}^{\infty}\binom{2n+1}{m}\frac{(-1)^n\,\alpha^m\beta^{2n+1-m}}{n!\,(2n+1)\,(2n+1-m)}\left(e^{b(2n+1-m)}-e^{a(2n+1-m)}\right). \tag{7.4}$$

$$\int_a^b Q\left(\alpha+\beta e^{x}\right)dx=\frac{b-a}{2}-\frac{1}{\sqrt{\pi}}\sum_{n=0}^{\infty}\sum_{m=0}^{\infty}\binom{2n+1}{m}\frac{2^{\frac{-(2n+1)}{2}}\,(-1)^n\,\alpha^m\beta^{2n+1-m}}{n!\,(2n+1)\,(2n+1-m)}\left(e^{b(2n+1-m)}-e^{a(2n+1-m)}\right). \tag{7.5}$$

For simplicity, we replace τ_{0A} with τ

$$\int_\omega^\gamma Q\left(\alpha+\beta e^{\frac{-\tau}{\tau_{rms}}}\right)d\tau=\frac{\gamma-\omega}{2}+\frac{\tau_{rms}}{\sqrt{\pi}}\sum_{n=0}^{\infty}\sum_{m=0}^{\infty}\binom{2n+1}{m}\frac{2^{\frac{-(2n+1)}{2}}\,(-1)^n\,\alpha^m\beta^{2n+1-m}}{n!\,(2n+1)\,(2n+1-m)}\left(e^{\frac{-\gamma(2n+1-m)}{\tau_{rms}}}-e^{\frac{-\omega(2n+1-m)}{\tau_{rms}}}\right). \tag{7.6}$$

In the special case when $\gamma = T_s$ and $\omega = 0$ we have

$$\int_0^{T_s} Q\left(\alpha + \beta e^{\frac{-\tau}{\tau_{rms}}}\right) d\tau = \frac{T_s}{2} + \frac{\tau_{rms}}{\sqrt{\pi}} \sum_{n=0}^{\infty} \sum_{m=0}^{\infty} \binom{2n+1}{m} \frac{2^{\frac{-(2n+1)}{2}} (-1)^n \alpha^m \beta^{2n+1-m}}{n! (2n+1) (2n+1-m)} \left(e^{\frac{-T_s(2n+1-m)}{\tau_{rms}}} - 1\right). \tag{7.7}$$

Hence

$$E\left[Q\left(\alpha + \beta e^{\frac{-\tau}{\tau_{rms}}}\right)\right] = \frac{1}{2} + \frac{\tau_{rms}}{T_s\sqrt{\pi}} \sum_{n=0}^{\infty} \sum_{m=0}^{\infty} \binom{2n+1}{m} \frac{2^{\frac{-(2n+1)}{2}} (-1)^n \alpha^m \beta^{2n+1-m}}{n! (2n+1) (2n+1-m)} \left(e^{\frac{-T_s(2n+1-m)}{\tau_{rms}}} - 1\right). \tag{7.8}$$

Bibliography

[1] F. Shang, B. Champagne, and I. N. Psaromiligkos, "A ML-based framework for joint TOA/AOA estimation of UWB pulses in dense multipath environments," *IEEE Trans. Wireless Commun.*, vol. 13, no. 10, pp. 5305–5318, Oct. 2014.

[2] V. Kristem, A. F. Molisch, S. Niranjayan, S. Sangodoyin, "Coherent UWB ranging in the presence of multiuser interference," *IEEE Trans. Wireless Commun.*, vol. 13, no. 8, pp. 4424–4439, Aug. 2014.

[3] Z. Xiao, H. Wen, A. Markham, N. Trigoni, P. Blunsom, and J. Frolik,, "Non-line-of-sight identification and mitigation using received signal strength," *IEEE Trans. Wireless Commun.*, vol. 14, no. 3, pp. 1689–1702, Mar. 2015.

[4] V. Savic, E. Larsson, and J. Ferrer-Coll, and P. Stenumgaard, "Kernel methods for accurate UWB-based ranging with reduced complexity," *IEEE Trans. Wireless Commun.* no. 99, pp. 1–1, Oct. 2015.

[5] S. Li, R. C. De Lamare, and M. Haardt, "Adaptive frequency-domain group-based shrinkage estimators for UWB systems," *IEEE Trans. Veh. Technol.*, vol. 62, no. 8, pp. 3639–3652, Oct. 2013.

[6] T. Wang, T. Lv, H. Gao, and Y. Lu, "BER analysis of decision-feedback multiple-symbol detection in noncoherent MIMO ultrawideband systems," *IEEE Trans. Veh. Technol.*, vol. 62, no. 9, pp. 4684–4690, Nov. 2013.

[7] M. Z. Win and R. A. Scholtz, "Impulse radio: how it works," *IEEE Commun. Lett.*, vol. 2, no. 2, pp. 36–38, 1998

[8] L. Yang and G. B. Giannakis, "Ultra-wideband communications: an idea whose time has come," *IEEE Signal Process. Mag.*, vol. 21, no. 6, pp. 26–54, Nov. 2004

[9] IEEE Std 802.15.3TM 2003, -Part 15.3: Specifications for High Rate Wireless Personal Area Networks (WPANs).

[10] IEEE Std 802.15.4TM 2006, -Part 15.4: Specifications for Low- Rate Wireless Personal Area Networks (WPANs).

[11] WiMedia Radio: Current Regulatory Status and Respective Industry Positions, August 2008

[12] A. Tanaka, H. Okada, H. Kadama, H. Ishikawa, "A 1.1V 3.1-9.5GHz MB-OFDM UWB transceiver in 90nm CMOS," in *Proc. IEEE Int. Conf. Solid-State Circuits*, 2006, pp. 398–407.

[13] D. Leenarts, et al, "A 65nm CMOS inductorless triple-band-group WiMedia UWB PHY," in *Proc. IEEE Int. Conf. Solid-State Circuits*, 2009, pp. 410–411.

[14] E. Juntunen, et al., "A 33pJ/bit 90nm CMOS UWB single-chip transceiver with embedded multi-gigabit modem," in *Proc. IEEE Int. Microwave Symp.*, 2009, pp. 1–4.

[15] M. Nejad, et al., "A remote-powered RFID tag with 10Mb/s UWB uplink and -18.5dBm sensitivity UHF downlink in 0.18um CMOS," in *Proc. IEEE Int. Solid-State Circuits Conf.*, 2009, pp. 198–200.

[16] R. J. Fontana, E. Richley, J. Barney, "Commercialization of an ultra wideband precision asset location system," in *Proc. IEEE Conf. Ultra Wideband Sys. and Technol.*, 2003. pp. 369–373.

[17] Y. Zheng, M. Arasu, K. Wong, Y. The, A. Suan, D. Tran, W. Yeoh, and D. Kwong, "A 0.18um CMOS 802.15.4a UWB transceiver for communication and localization," in *Proc. IEEE Int. Conf. Solid-State Circuits*, 2008. pp. 118–119.

[18] T. Kikkawa, P. Saha, N. Sasaki, K. Kimoto, "Gaussian monocycle pulse transmitter using 0.18um CMOS technology with on-chip integrated antennas for inter-chip UWB communication," *IEEE J. Solid-State Circuits*, vol. 43, no. 5, pp. 1303–1312, May 2008.

[19] N. Sasaki, et al., "A single-chip ultra-wideband receiver with silicon integrated antennas for inter-chip wireless interconnection," *IEEE J. Solid-State Circuits,* vol. 44, no. 2, pp. 382–393, Feb. 2009.

[20] Y. Wang, A. Niknejad, V. Gaudet, and K. Iniewski "A CMOS IR-UWB transceiver design for contact-less chip testing applications," *IEEE Trans. Circuits and Systems*, vol. 55, no. 4, pp. 334–338, Apr. 2008.

[21] M. Chae, W. Liu, Z. Yang, T. Chen, J. Kim, M. Sivaprakasam, and M. Yuce, "A 128-channel 6mW wireless neural recording IC with on-the-fly spike sorting and UWB transmitter," in *Proc. IEEE Int. Conf. Solid-State Circuits*, 2008. pp. 146–147.

[22] O. Novak and C. Charles, "Low-power UWB pulse generators for biomedical implants," in *Proc. IEEE Int. conf. Ultra-Wideband*, 2009, pp. 778–782.

[23] T. Chu and H. Hashemi, "A CMOS UWB camera with 7x7 simultaneous active pixels," in *Proc. IEEE Int. Conf. Solid-State Circuits*, Feb. 2008, pp. 120–121.

[24] A. F. Molisch, K. Balakrishnan, D. Cassioli, C. Chong, S. Emami, A. Fort, J. Karedal, J. Kunisch, H. Schantz, U. Schuster, and K. Siwiak, "IEEE 802.15.4a channel model final report," IEEE 802.15.4a, Tech. Rep., 2005. Available (Online): `http://grouper.ieee.org/groups/802/15/pub/04/15-04-0662-02-004achannel-model-final-report-r1.pdf`

[25] Federal Communications Commission, "First Report and Order 02-48," Feb. 2002.

[26] G. Breed, "A summary of FCC rules for ultra wideband communications," *High Frequency Electronics,* Jan.2005. [Online]. Available: `http://www.highfrequencyelectronics.com/Archives/Jan05/HFE0105_Tutorial.pdf`

[27] M. Basaran, S. Erkucuk, and H. A. Cirpan, "The effect of channel models on compressed sensing based UWB channel estimation," in *Proc. IEEE Int. Conf. Ultra-Wideband,* 2011, pp. 375–379.

[28] M. Ozgor, S. Erkucuk, and H. A. Cirpan, "Bayesian compressive sensing for ultra-wideband channel models," in *Proc. Int. Conf. Telecommun. and Signal Process.*, Jul. 2012. pp. 320–324.

[29] H. Rauhut, K. Schnass, and P. Vandergheynst, "Compressed sensing and redundant dictionaries," *IEEE Trans. Inf. Theory*, vol. 54, no. 5, pp. 2210–2219, 2008.

[30] E. Cand'es and J. Romberg, "Sparsity and incoherence in compressive sampling," Inverse Problems, vol. 23, pp. 969, 2007.

[31] M. Akcakaya and V. Tarokh, "Shannon-theoretic limits on noisy compressive sampling," *IEEE Trans. Inf. Theory*, vol. 56, no. 1, pp. 492–504, Jan. 2010.

[32] W. U. Bajwa, J. Haupt, A. M. Sayeed, and R. Nowak, "Compressed channel sensing: a new approach to estimating sparse multipath channels," *Proceedings of IEEE*, vol. 98, pp. 1058–1076, Jun. 2010.

[33] M. Vetterli, P. Marziliano, and T. Blu, "Sampling signals with finite rate of innovation," *IEEE Trans. Signal Process.*, vol. 50, no. 6, pp. 1417–1428, Jun. 2002.

[34] P. L. Dragotti, M. Vetterli, and T. Blu, "Sampling moments and reconstructing signals of finite rate of innovation: shannon meets strang fix," *IEEE Trans. Signal Process.*, vol. 55, no. 5, pp. 1741–1757, May 2007.

[35] G. Marjanovic and V. Solo, "On ℓ_q Optimization and sparse inverse covariance selection," *IEEE Trans. Signal Process.*, vol. 62, no. 7, pp. 1644–1654, Apr. 2014.

[36] B. Mulgrew, "The stationary phase approximation, time-frequency decomposition and auditory process.," *IEEE Trans. Signal Process.*, vol. 62, no. 1, pp. 56–68, Jan. 2014.

[37] X. Rao and V. K. N. Lau, "Distributed compressive CSIT estimation and feedback for FDD multi-user massive MIMO systems," *IEEE Trans. Signal Process.*, vol. 62, no. 12, pp. 3261–3271, Jun. 2014.

[38] T. Tsiligkaridis, A. O. Hero, and S. Zhou, "On convergence of kronecker graphical lasso algorithms," *IEEE Trans. Signal Process.*, vol. 61, no. 7, pp. 1743–1755, Apr. 2013.

[39] A. Benichoux, L. S. R. Simon, E. Vincent, and R. Gribonval, "Convex regularizations for the simultaneous recording of room impulse responses," *IEEE Trans. Signal Process.*, vol. 62, no. 8, pp. 1976–1986, Apr. 2014.

[40] P. Y. Chen and I. W. Selesnick, "Group-sparse signal denoising: non-convex regularization, convex optimization," *IEEE Trans. Signal Process.*, vol. 62, no. 13, pp. 3464–3478, Jul. 2014.

[41] T. Peleg, Y. C. Eldar, and M. Elad, "Exploiting statistical dependencies in sparse representations for signal recovery," *IEEE Trans. Signal Process.*, vol. 60, no. 5, pp. 2286–2303, May 2012.

[42] E. Vural and P. Frossard, "Learning smooth pattern transformation manifolds," *IEEE Trans. Image Proc.*, vol. 22, no. 4, pp. 1311–1325, Apr. 2013.

[43] X. Fang, Y. Xu, X. Li, Z. Lai, and W. K. Wong, "Learning a nonnegative sparse graph for linear regression," *IEEE Trans. Image Process.*, vol. 24, no. 9, pp. 2760–2771, Sep. 2015.

[44] X. Xu, Z. Hou, C. Lian, and H. He, "Online learning control using adaptive critic designs with sparse kernel machines," *IEEE Trans. Neural Networks and Learning Systems*, vol. 24, no. 5, pp. 762–775, May 2013.

[45] Z. Tan, P. Yang, and A. Nehorai, "Joint sparse recovery method for compressed sensing with structured dictionary mismatches," *IEEE Trans. Signal Process.*, vol. 62, no. 19, pp. 4997–5008, Oct. 2014.

[46] A. Liu and V. Lau, "Joint interference mitigation and data recovery in compressive domain: a sparse MLE approach," *IEEE Trans. Signal Process.*, vol. 62, no. 19, pp. 5184–5195, Oct. 2014.

[47] R. He, W. S. Zheng, B. G. Hu, and X. W. Kong, "Two-stage nonnegative sparse representation for large-scale face recognition," *IEEE Trans. Neural Networks and Learning Systems*, vol. 24, no. 1, pp. 35–46, Jan. 2013.

[48] J. Ren, J. Liu, and Z. Guo, "Context-aware sparse decomposition for image denoising and super-resolution," *IEEE Trans. Image Process.*, vol. 22, no. 4, pp. 1456–1469, Apr. 2013.

[49] Y. Han, F. Wu, Q. Tian, and Y. Zhuang, "Image annotation by input-output structural grouping sparsity," *IEEE Trans. Image Process.*, vol. 21, no. 6, pp. 3066–3079, Jun. 2012.

[50] R. DeVore. Nonlinear approximation. *Acta Numerica*, 7:51–150, 1998.

[51] J. L. Paredes, G. R. Arce, and Z. Wang, "Ultra-wideband compressed sensing: channel estimation," *IEEE J. Selected Topics in Signal Process.*, vol. 1, pp. 383–395, Oct. 2007.

[52] M. Ozgor, S. Erkucuk, and H. A. Cirpan, "Bayesian compressive sensing for ultra-wideband channel models," in *Proc. Int. Conf. Telecommun. and Signal Process.*, 2012, pp. 320–324.

[53] S. Chen, D. Donoho, and M. Saunders, "Atomic decomposition by basis pursuit," *SIAM J. Sci. Comp.*, vol. 20, pp. 33–61, 1998.

[54] D. Morton de Lachapelle, D. Gfeller, and P. De LOS Rios, "Shrinking matrices while preserving their eigenpairs with application to the spectral coarse graining of graphs" *SIAM J. Matrix Analysis and Applications,* 2008.

[55] S. J. Kim, K. Koh, M. Lustig, S. Boyd, and D. Gorinevsky, "An interior-point method for large-scale ℓ_1 regularized least squares," *IEEE J. Signal Process.*, vol. 1, no. 4, pp. 606–617, Dec. 2007.

[56] A. Y. Yang, S. S. Sastry, A. Ganesh, and Yi Ma, "Fast ℓ_1-minimization algorithms and an application in robust face recognition: a review," in *Proc. IEEE Int. Conf. Image Process.*, 2010. pp. 1849–1852.

[57] L. Mucchi, E. D. Re, and T. Landi, "Multi-level environment identification method for impulsive radio systems," in *Proc. IEEE Int. Conf. Ultra-Wideband*, 2011, pp. 385–389.

[58] N. Decarli, D. Dardari, S. Gezici, and A. A. D'Amico, "LOS/NLOS detection for UWB signals: A comparative study using experimental data," in *Proc. IEEE Int. Symp. Wireless Pervasive Computing*, 2010, pp. 169–173.

[59] S. Venkatesh and R. M. Buehrer, "NLOS mitigation using linear programming in ultrawideband location-aware networks," *IEEE Trans. Veh. Technol.*, pp. 3182–3198. Sept. 2007.

[60] N. Alsindi, C. Duan, J. Zhang, and T. Tsuboi, "LOS channel identification and mitigation in ultra wideband TOA-based wireless sensor networks," *Workshop Positioning, Navigation and commun.*, 2009, pp. 59–66.

[61] I. Guvenc, C. C. Chong, and F. Watanabe, "NLOS identification and mitigation for UWB localization Systems," in *Proc. IEEE Conf. Wireless commun. and Networking*, 2007, pp. 1571–1576.

[62] A. Abbasi and M. H. Kahaei, "Improving source localization in LOS and NLOS multipath environments for UWB signals," in *Proc. IEEE Int. CSI Computer Conf.*, 2009, pp. 310–316.

[63] L. Mucchi and P. Marcocci, "A new parameter for UWB indoor channel profile identification," *IEEE Trans. Wireless Commun.*, vol. 8, no. 4, pp. 1597–1602. Apr. 2009.

[64] M. Guerra and A. Conti "Experimental multilevel NLOS characterization for UWB network localization," *IEEE Workshop Statistical Signal Process.*, 2011, pp. 173–176.

[65] G. Bellusci, G. Janssen, J. Yan, and C. Tiberius, "Model of distance and bandwidth dependency of TOA-based UWB ranging error," in *Proc. IEEE Int. Conf. Ultra-Wideband*, vol. 3, 2008, pp. 193–196.

[66] H. Chen, G. Wang, Z. Wang, H. C. So, and H. V. Poor, "Non-line-of-sight node localization based on semi-definite programming in wireless sensor networks," *IEEE Trans. Wireless Commun.*, vol. 11, no. 1, pp. 108–116. Jan. 2012.

[67] S. Y. Cho and Y. W. Choi, "Access point-less wireless location method based on peer-to-peer ranging of impulse radio ultra-wideband," *IET Radar, Sonar and Navigation*, vol. 4, no. 4, pp. 733–743, Oct. 2010.

[68] B. Shen, R. Yang, S. Ullah, and K. Kwak, "Linear quadrature optimisation-based non-coherent time of arrival estimation scheme for impulse radio ultra-wideband systems," *IET Commun.*, vol. 4, no. 12, pp. 1471–1483, Aug. 2010.

[69] J. Xu, M. Ma, and C. L. Law, "Performance of time-difference-of-arrival ultra wideband indoor localisation," *IET Science, Measurement and Tech.*, vol. 5, no. 4, pp. 46–53, Mar. 2011.

[70] Z. Irahhauten, H. Nikookar, and M. Klepper, "A joint ToA/DoA technique for 2D/3D UWB localization in indoor multipath environment," in *Proc. IEEE Int. Conf. Commun.*, 2012, pp. 4499–4503.

[71] O. Abdul-Latif, P. Shepherd, and S. Pennock, "TDOA/AOA data fusion for enhancing positioning in an ultra wideband system," in *Proc. IEEE Int. Conf. Signal Process. and Commun.*, 2007, pp. 1531–1534.

[72] M. H. Kabir and R. Kohno, "A hybrid positioning approach by UWB radio communication systems for non line-of-sight conditions," in *Proc. IEEE Global Telecommun. Conf.*, 2011.

[73] M. F. Hanif, P. J. Smith, and P. A. Dmochowski, "Statistical interference modelling and deployment issues for cognitive radio systems in shadow fading environments," *IET Commun.*, vol. 6, no. 13, pp. 1920–1929. Sept. 2012.

[74] M. Segura, V. Mut, and C. Sisterna, "Ultra wideband indoor navigation system," *IET Radar, Sonar and Navigation*, vol. 6, no. 5, pp. 402–411. Jun. 2012.

[75] L. Zao and R. Coelho, "Generation of coloured acoustic noise samples with non-Gaussian distributions," *IET Signal Process.*, vol. 6, no. 7, pp. 684–688, Sep. 2012.

[76] M. Zeddam, A. F. Moulin, and F. Gauthier, "Indoor power-line communications channel characterization up to 100 MHz Part II: time-frequency analysis," *IEEE Trans. Power Del.*, vol. 23, no. 3, pp. 1402–1409, Jul. 2008.

[77] J. Y. Lee, Y. H. Jo, S. H. Kang, A. Y. Kang, D. H. Ha, and, S. J. Yoon, "Determination of the existence of LOS blockage and its application to UWB localization" in *Proc. IEEE Conf. Military Commun.*, 2006, pp. 1–4.

[78] S. Wu, Q. Zhang, Q. Zhang, and H. Yao, "Integrative ranging and positioning for IR-UWB wireless sensor networks," in *Proc. Int. Conf. Commun. and Mobile Computing*, 2011, pp. 489–494.

[79] P. K. Dash, K. R. Krishnanand, and M. Padhee, "Fast recursive Gauss-Newton adaptive filter for the estimation of power system frequency and harmonics in a noisy environment," *IET Generation, Transmission and Distribution*, vol. 5, no. 12, pp. 1277–1289, Dec. 2011.

[80] K. Yu and Y. J. Guo, "Improved positioning algorithms for NLOS environments," *IEEE Trans. Veh. Technol.*, vol. 57, no. 4, pp. 2342–2353, Jul. 2008.

[81] E. Karapistoli, F. N. Pavlidou, I. Gragopoulos, and I. Tsetsinas, "An overview of the IEEE 802.15.4a standard," *IEEE Commun. Mag.*, vol. 48, pp. 47–53, Jan. 2010.

[82] S. Yang and Q. Zhao, "Probability distribution characterisation of fault detection delays and false alarms," in *Proc. IET Cont. Theory and App.*, vol. 6, no. 7, pp. 953–962, May 2012.

[83] M. Hamdi, J. Mietzner, and R. Schober, "Multiple-differential encoding for multi-hop amplify-and-forward IR-UWB systems," *IEEE Trans. Wireless Commun.*, vol. 10, no. 8, pp. 2577–2591, 2011.

[84] Z. Zeinalpour-Yazdi, M. Nasiri-Kenari, and B. Aazhang, "Performance of UWB linked relay network with time-reversed transmission in the presence of channel estimation error," *IEEE Trans. Wireless Commun.*, vol. 11, no. 8, pp. 2958–2969, Aug. 2012.

[85] M. Mondelli, Q. Zhou, X. Ma, and V. Lottici, "A cooperative approach for amplify-and-forward differential transmitted reference IR-UWB relay systems," in *Proc. IEEE Int. Conf. Acoustics, Speech and Signal Process.*, pp. 2905–2908, Mar. 2012.

[86] M. Mondelli, Q. Zhou, V. Lottici, and X. Ma, "Joint power allocation and path selection for multi-hop noncoherent decode and forward UWB communications," *IEEE Trans. Wireless Commun.*, vol. 13, no. 3, pp. 1397–1409, Mar. 2014.

[87] C. Abou-Rjeily, "A symbol-by-symbol cooperative diversity scheme for relay-assisted UWB communications with PPM," *IEEE J. Sel. Areas Commun.*, vol. 31, no. 8, pp. 1436–1445, Aug. 2013.

[88] G. Pan, E. Ekici, and Q. Feng, "Performance Analysis of Cooperative Time Hopping UWB Systems with Multi-User Interference," *IEEE Trans. Wireless Commun.*, vol. 11, no. 6, pp. 1969–1975, Jun. 2012.

[89] Z. Ahmadian, L. Lampe, and J. Mietzner, "Multiuser two-way relaying schemes for UWB communication," *IEEE Trans. Wireless Commun.*, no. 99, pp. 1–1.

[90] Y. Dai, L. Pan, and X. Dong, "Physical-layer network coding aided bi-directional cooperative relays for transmitted reference pulse cluster UWB systems," in *Proc. IEEE Int. Conf. Commun.*, 2014. pp. 5825–5830.

[91] Z. Wang, T. Lv, H. Gao, and Y. Li, "A novel two-way relay UWB network with joint non-coherent detection in multipath," in *Proc. IEEE Veh. Technol. Conf.*, 2011. pp. 1–5.

[92] B. Rankov and A. Wittneben, "Spectral efficient signaling for half-duplex relay channels," in *Proc. Rec. 39th Asilomar Conf. Signals, Syst. Comput.*, pp. 1066–1071. 2005.

[93] T. J. Oechtering and H. Boche, "Bidirectional regenerative half-duplex relaying using relay selection," *IEEE Trans. Wireless Commun.*, vol. 7, no. 5, pp. 1879–1888, May 2008.

[94] L. Ding, M. Tao, F. Yang, and W. Zhang, "Joint scheduling and relay selection in one- and two-way relay networks with buffering," in *Proc. IEEE Int. Conf. Commun.*, pp. 1–5, 2009.

[95] P. Popovski and H. Yomo, "Wireless network coding by amplify-and-forward for bi-directional traffic flows," *IEEE Commun. Letters,* vol. 11, no. 1, pp. 16–18, Jan. 2007.

[96] S. Zhang, S. C. Liew, and P. P. Lam, "Physical-Layer Network Coding," *ACM MOBICOM*, Sept. 2006.

[97] P. Popovski and H. Yomo, ''Physical Network Coding in Two-Way Wireless Relay Channels," in *Proc. IEEE Int. Conf. Commun.*, 2007, pp. 707–712.

[98] E. C. Y. Peh, Y.-C. Liang, and Y. L. Guan, "Power Control for Physical-Layer Network Coding in Fading Environments, *IEEE Personal, Indoor and Mobile Radio Commun.* pp. 1–5, Sep. 2008.

[99] Y. Qiuna, Y. D. Wu, Y. He, "Cooperative Diversity of Wireless Networks with Multiple Amplify and Forward Relays," in *Proc. Int. Conf. Commun. and Mobile Computing*, pp. 207–212.

[100] P. Popovski and H. Yomo, "Bi-directional amplification of throughput in a wireless multi-hop network, in *Proc. IEEE Veh. Tech. Conf.* May 2006.

[101] P. Popovski and H. Yomo,"The Anti-Packets Can Increase the Achievable Throughput of a Wireless Multi-Hop Network," in *Proc. IEEE Int Conf Commun.*, pp. 3885–3890, Jun. 2006.

[102] T. Koike-Akino, P. Popovski, and V, Tarokh, "Optimized constellations for two-way wireless relaying with physical network coding," *IEEE J. Sel. Areas in Commun.* vol. 27, no. 5, pp. 773–787, Jun. 2009.

[103] J. Laneman, D. Tse, and G. Wornell, "Cooperative diversity in wireless networks: Efficient protocols and outage behavior," *IEEE Trans. Inf. Theory*, vol. 50, no. 12, pp. 3062–3080, Dec. 2004.

[104] A. Sendonaris, E. Erkip, and B. Aazhang, "User cooperation diversity. Part I. System description," *IEEE Trans. Commun.*, vol. 51, no. 11, pp. 1927–1938, Nov. 2003.

[105] A. Sendonaris, E. Erkip, and B. Aazhang, "User cooperation diversity. Part II. Implementation aspects and performance analysis," *IEEE Trans. Commun.*, vol. 51, no. 11, pp. 1939–1948, Nov. 2003.

[106] A. Bletsas, H. Shin, and M. Win, "Cooperative communications with outage-optimal opportunistic relaying," *IEEE Trans. Commun.*, vol. 6, no. 9, pp. 3450–3460, Sep. 2007.

[107] M. Dohler, Y. Li, B. Vucetic, A. H. Aghvami, M. Arndt, and D. Barthel, "Performance analysis of distributed space-time block-encoded sensor networks," *IEEE Trans. Veh. Technol.*, vol. 55, no. 6, pp. 1776–1789, Nov. 2006.

[108] G. Durisi and S. Benedetto, "Comparison between coherent and noncoherent receivers for UWB communications," *EURASIP J. Appl. Signal Process.*, pp. 359–368, 2005.

[109] K. Maichalernnukul, T. Kaiser, and F. Zheng, "On the performance of coherent and noncoherent UWB detection systems using a relay with multiple antennas," *IEEE Trans. Wireless Commun.*, vol. 8, no. 7, pp. 3407–3414, 2009.

[110] C. Cho, H. Zhang, and M. Nakagawa, "A short delay relay scheme using shared frequency repeater for UWB impulse radio," *IEICE Trans. Fundamentals of Electronics, Commun. and Computer Sciences*, vol. 90, no. 7, pp. 1444–1451, 2007.

[111] Z. Z. Yazdi, M. N. Kenari, and B. Aazhang, "Bit error probability analysis of UWB communications with a relay node," *IEEE Trans. Commun.*, vol. 9, no. 2, pp. 802–813, Feb. 2010.

[112] L. Yang, G. B. Giannakis, and A. Swami, "Noncoherent ultra-wideband (de)modulation," *IEEE Trans. Commun.*, vol. 55, no. 4, pp. 810–819, Apr. 2007.

[113] K. Witrisal and M. Pausini, "Statistical analysis of UWB channel correlation functions," *IEEE Trans. Veh. Technol.*, vol. 57, no. 3, pp. 1359–1373, May 2008.

[114] H. Gao, X. Su, T. Lv, T. Wang, and Z. Wang, "Physical-layer network coding aided two-way relay for transmitted-reference UWB networks," in *Proc. IEEE Global Telecommun. Conf.* pp. 1–6. Dec. 2011.

[115] B. Rankov and A. Wittneben, "Spectral efficient protocols for halfduplex fading relay channels," *IEEE J. Select. Areas Commun.*, vol. 25, no. 2, pp. 379–389, Feb. 2007.

[116] R. Louie, Y. Li, and B. Vucetic, "Practical physical layer network coding for two-way relay channels: performance analysis and comparison," *IEEE Trans. Wireless Commun.*, vol. 9, no. 2, pp. 764–777, Feb. 2010.

[117] X. Dong and X. Dong, "Bi-directional cooperative relays for transmitted reference pulse cluster UWB systems," in *Proc. IEEE Conf. Global Telecommu.*, pp. 1–5. Dec. 2010.

[118] Z. Wang, T. Lv, H. Gao, and Y. Li, "A novel two-way relay UWB network with joint non-coherent detection in multipath," in *Proc. IEEE Conf. Veh. Tech.*, pp. 1–5. May 2011.